

EXPOSURE OF NEARSHORE ORGANISMS TO CLIMATE STRESSORS IN THE
UPWELLING REGION OF MONTEREY BAY

by

MATHEUS FAGUNDES

(Under the Direction of C. Brock Woodson)

ABSTRACT

Climate change is expected to warm, deoxygenate, and acidify ocean waters in the future. However, nearshore ecosystems are affected by a range of processes such as tides, local winds, internal and surface waves, that cause variability in climate stressors that can be greater than the change predicted by global climate models. A 2D implementation of the Regional Ocean Modeling System (ROMS) to downscale global climate predictions to the scale of a local reef for all Representative Concentration Pathway (RCP) scenarios. I found that exposure to climate stressors (temperature, pH, dissolved oxygen) increases as carbon emissions pathways increase as expected. Significant exposure is generally not expected until RCP 4.5 or greater for temperature and pH, while oxygen exposure is already occurring. Observed variability also is expected to increase in future climate scenarios and may act as a mitigating factor in the future.

INDEX WORDS : Climate change, warming, hypoxia, ocean acidification, ocean modeling, multiple stressors

EXPOSURE OF NEARSHORE ORGANISMS TO CLIMATE
STRESSORS IN THE UPWELLING REGION OF MONTEREY BAY

by

MATHEUS FAGUNDES

B.S., Universidade Federal do Maranhao (UFMA), Brazil, 2016

A Thesis Submitted to the Graduate Faculty of The University of Georgia
in Partial Fulfillment of the Requirements for the Degree

MASTER OF MARINE SCIENCES

ATHENS, GEORGIA

2018

© 2018

Matheus Fagundes

All Rights Reserved

EXPOSURE OF NEARSHORE ORGANISMS TO CLIMATE
STRESSORS IN THE UPWELLING REGION OF MONTEREY BAY

by

MATHEUS FAGUNDES

Major Professor: C. Brock Woodson

Committee: Patricia M. Medeiros

Renato M. Castelao

Electronic version Approved:

Suzanne Barbour

Dean of the Graduate School

The University of Georgia

December 2018

ACKNOWLEDGMENTS

First of all, I think my gratitude and acknowledgments should start by saying thank you to my advisor, Brock Woodson, for believing in that undergraduate Brazilian student from a not known university. My gratitude is even greater when I think about the moments of frustration over modeling and how he helped me handling it by showing me a different perspective. Of course, how patient he was to try to figure it out what my problem was when I did not know how to explain it in English. My other thank you is for NSF for sponsoring Brock's idea and therefore hiring me to this position.

I also would like to say thank you for my labmates Ben Hefner and Soroush Omidvar for talking to me and showing me different views based on their culture, and for the moments of laugh and fun. Another special thank you is for my girlfriend who tried really hard to understand and support what I did for my masters. I would also like to thank my friends for all the Thursdays night at Cutters that we talked about among other things our work.

The last but really special gratitude is towards my family (my mother, my father, my sisters). I remember the times my father said that I should learn English because it would help me in my career. Even though, I failed one semester (he does not know that) I was able to achieve what I was looking forward since I was a kid... to study and work hard so one day I could give a better life for my parents. I still have a long path to go so I can help my parents, though. Finally, I would like to dedicate this last sentence to my grandmother who made a promise that if my mom did not abort me (because of health problems with her pregnancy), my grandmother would raise me until I was 5. Unfortunately, I won't be able to say thank to her for believing in me since I was in the belly of my mom and still believed me and always made me the best example for my cousins. This thanks is not going to be in person since you passed away last year, vo Santa, but I will be always thankful for

everything especially all the delicious foods you always made for me every time I went to your house. Sorry for not being there when you left us.

Contents

ACKNOWLEDGMENTS	iv
LIST OF FIGURES	vii
LIST OF TABLES	ix
1 Introduction and Motivation	1
1.1 Background	3
1.2 Goals	10
2 FORECASTING EXPOSURE OF NEARSHORE ECOSYSTEMS TO CLIMATE CHANGE IMPACTS	11
2.1 Introduction	13
2.2 Monterey Bay configuration	16
2.3 Data	23
2.4 Analysis	34
2.5 Results	38
2.6 Discussion	50
2.7 Conclusions	55
3 Final Remarks and Future directions	56
BIBLIOGRAPHY	57

List of Figures

1.1	Semi-Permanent Pressure Systems for January and July.	5
1.2	Subdivision of California Current system (CCS) and its major processes. From Checkley and Barth (2009).	7
2.1	Model domain based on the cross shore section (red line).	17
2.2	Vertical view of the domain based on Walter et al. (2014).	19
2.3	Sea breeze and downwelling winds time series used for the simulation.	24
2.4	Time series used for shortwave radiation.	26
2.5	Time Series of velocity used to force West boundary in the model.	27
2.6	Schematic of tidal currents subduction and vertical velocity profile at the site of study.	28
2.7	Initial and Boundary Conditions profiles for present and future scenarios: a) Temperature, b)O ₂ , c)DIC, d)pH.	32
2.8	Time series of temperature, Dissolved Oxygen, and pH from Booth et al. (2012) showing for a typical period of upwelling.	35
2.9	Power spectra of temperature (a), oxygen (b), and pH (c) from data used in (Booth et al., 2012) and current model showing model reproduces observed semi-diurnal and diurnal variability. Solid blue line represents the mean and the confidence intervals for the <i>in situ</i> data is represented by the blue line and shading, while solid red line represents our model output data with its confidence intervals (red shading). Data and model means are also shown.	39
2.10	Snapshot of u-component of velocity and temperature on July, 6th 2013 from the model. Positive values are onshore, negative values are offshore. Contour lines (black) show isotherms with temperature labels.	41

2.11	Modelled time series of Temperature for 1 month period with idealized upwelling for present day (a), RCP2.6 (b), RCP4.5 (c), RCP6.0 (d), and RCP8.5 (e).	42
2.12	Modeled time series of O ₂ for 1 month period with idealized upwelling resent day (a), RCP2.6 (b), RCP4.5 (c), RCP6.0 (d), and RCP8.5 (e).	43
2.13	Modeled time series of pH for 1 month period with idealized upwelling Present day (a), RCP2.6 (b), RCP4.5 (c), RCP6.0 (d), and RCP8.5 (e).	44
2.14	Integrated spectral daily variability for Temperature, DO, and pH. The y-axis gives the temperature, DO, and pH and the x-axis represents the scenarios. Red lines give the median of temperature, DO, and pH for each scenario. Whiskers represent the 95% confidence interval estimated using spectral analysis.	46
2.15	Bootstrap of the mean daily integrated exposure of temperature (a), dissolved oxygen (b), and acidification (c) from present and future scenarios for red abalone (<i>Haliotis rufescens</i>) and sea urchin (<i>Paracentrotus lividus</i> and <i>Mesocentrotus franciscanus</i>). Box plots show mean, 25% and 75% quantiles, and data range.	48

List of Tables

2.1	Boundary Conditions for the domain.	20
2.2	Boundary Conditions for the Biological tracers.	21
2.3	Initial settings for the Idealized case.	22
2.4	Values for present and future scenarios at surface and bottom used to fit the equation and used as Boundary condition for the Idealized experiment.	31
2.5	Final values for present and future scenarios at bottom found by fitting the equation and used as Initial and Boundary conditions for the Idealized experiment.	33
2.6	Threshold for fertilization and grazing success of two benthic taxa in the CCS.	36
2.7	Comparison different scenarios of accumulative exposure to acidification and hypoxia during a period of a week for <i>H. rufescens</i>	53

Chapter 1

Introduction and Motivation

Higher temperatures, hypoxia, and ocean acidification are all major consequences of climate change for the world's oceans (Bopp et al., 2013; Resplandy et al., 2013; Gobler and Baumann, 2016). Large scale changes in atmospheric CO₂ and the resulting impacts on the ocean are ultimately translated into regional (Xiu et al., 2018) and local scale stresses on ecosystems (Woodson, 2018). Laboratory experiments on the effects of climate change stressors are generally static with constant values of temperature, oxygen content, or pH, and therefore, they do not accurately represent the multi-stress vulnerability that organisms deal in real environments (Cressey, 2015). In many nearshore ecosystems, the variability in temperature, oxygen and pH is greater than the expected change due to future climate. Studies of exposure and response of nearshore organisms to climate impacts in these highly variable environments with multiple stressors are beginning to be studied in the laboratory (Boch et al., 2018; Low and Micheli, 2018). Thus, a more realistic representation of how climate change will manifest at the scale of a local ecosystem is needed. This study aims to understand how exposure to climate stressors varies in nearshore ecosystems of Monterey Bay, CA, and highlights the potential consequences for two model species. The primary goals of this thesis are:

- **Goal 1:** Determine how variability of pH, DO, and temperature during the upwelling season are going to change in the future.
- **Goal 2:** Quantify the exposure of organisms to hypoxic, acidification, and warmer waters in upwelling regions for various climate change scenarios.

And with these goals in mind, the specific objectives are:

- **Objective 1:** To build an idealized coupled hydrodynamic-biogeochemical model for Monterey Bay, CA.
- **Objective 2:** To examine different scenarios of climate change for the year 2100 using Representative Concentration Pathway (RCP) projections in the model.

Finally, I will use the model to address two hypotheses concerning the exposure of nearshore ecosystems to climate stressors:

- **Hypothesis 1:** Daily variability of pH, DO, and temperature during the upwelling season are going to be stronger in the future.
- **Hypothesis 2:** Climate change scenarios will increase the exposure of organisms to low oxygen, low pH waters due the intensification of hypoxia and increased acidification in upwelling regions.

1.1 Background

Climate change is expected to increase water temperature, reduce dissolved oxygen, and decrease ocean pH due to increases in anthropogenic CO₂. These changes occur at the global scale where they are affected by basin-scale circulation dynamics. Ultimately, the basin-scale conditions translate to local scales during which they are affected by a range of processes including wind-driven upwelling, internal tides, mixing, and biological processes (primary production, respiration). In this section, I start with the largest scales that will set the conditions expected under climate change (e.g. the Pacific Basin) and subsequently move down in scale to the California Current and upwelling dynamics to nearshore processes affecting temperature, oxygen and pH variability that animals will ultimately experience.

1.1.1 Pacific Ocean

The Pacific Ocean is the largest body of water on Earth (Talley et al., 2011). In the North Pacific, the circulation is mainly driven by winds causing a cyclonic circulation around the basin (Tsujino and Suginohara, 1998). The western and eastern boundary currents are fed by the subtropical gyre in the North Pacific. Along the eastern boundary, equatorward winds also drive intense upwelling that brings cold nutrient-rich waters to the surface. The eastern boundary of the North Pacific is represented by the Alaska Current System and the California Current System (CCS) (Nelson, 1976; Talley et al., 2011). As the global ocean uptakes CO₂, the Pacific Ocean is experiencing warming, expansion of oxygen minimum zones, and ocean acidification (Deutsch et al., 2011; Hofmann et al., 2011; Bopp et al., 2013; Feely et al., 2018).

1.1.2 California Current System (CCS)

The California Current is a bifurcation of the North Pacific gyre that carries 10 Sv equatorward year-round in the upper 500m (Checkley and Barth, 2009; Gangopadhyay et al., 2011; Talley et al., 2011). The CCS is composed of 3 main water masses: Pacific Subarctic water, North Pacific Central water, and Southern water (Marchesiello et al., 2003), where the

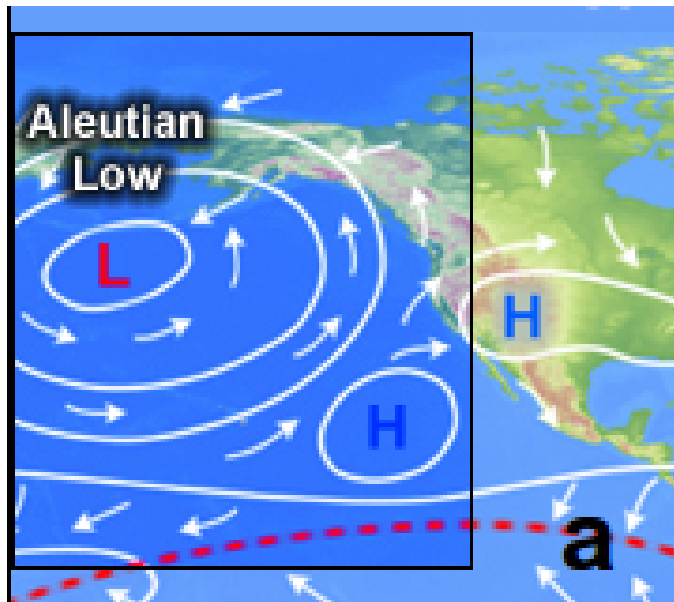
Pacific Subarctic water mass is carried southward by equatorward flow (Marchesiello et al., 2003). The CCS is mainly driven by large-scale winds associated with atmospheric pressure systems that vary seasonally (Huyer, 1983; Checkley and Barth, 2009). The interaction of Aleutian Low and North Pacific high pressure systems throughout the year affects different regions of CCS (Figure 1.1). For example, North Pacific high has more influence on the Central and Southern regions of CCS by increasing the intensity of equatorward winds causing seasonal wind-driven upwelling during spring and summer seasons (Kämpf and Chapman, 2016).

1.1.3 Upwelling

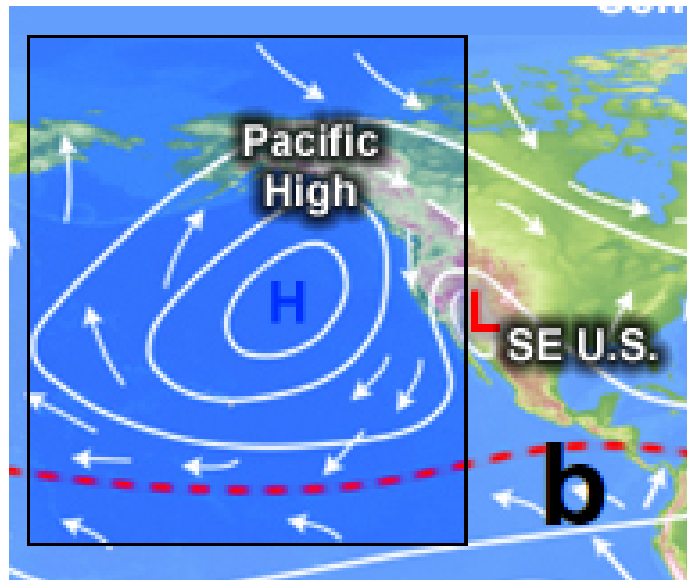
The intensification of equatorward winds during spring and summer seasons interacting with coastal topography and Earth’s rotation generates Ekman drift (Kämpf and Chapman, 2016). Ekman drift causes offshore net volume transport (Ekman transport) in the surface Ekman layer which is caused by interaction of Coriolis effect and wind stress and can be quantified as:

$$M = \frac{\tau}{\rho_{sw} |f|}$$

In order to maintain balance through the conservation of mass, cold and nutrient rich waters are upwelled to the surface close to the shore (Chavez and Messié, 2009; García-Reyes et al., 2015). These cold, nutrient rich waters are also low in dissolved oxygen and have low pH. The maximum horizontal gradient in water density occurs when these upwelled waters reach the surface creating upwelling fronts (Figure 1.2). Alongshore currents associated with upwelling fronts are responsible for intensifying the California Current during spring and summer (Huyer, 1983; Kämpf and Chapman, 2016). These upwelling jets are rich in nutrients with a unique biological zone (Kämpf and Chapman, 2016). Within the California Current, there are three distinct zones, the Northern, Central, and Southern regions (Checkley and Barth, 2009). The region of the most intense upwelling happens in the Central region of the CCS where it known as an Eastern Boundary Upwelling Ecosystem (EBUE’s) (Chavez and Messié, 2009). Monterey Bay, the focus of this study is located in the Central CCS.



(a) January.



(b) July.

Figure 1.1: Semi-Permanent Pressure Systems for January and July.

[Modified from: <http://ftp.comet.ucar.edu/oow/afwa/climo/intro/print.htmwelcome>]

When upwelling flow encounters a topographic feature, it may bifurcate into two jets. For example, topographic features lead to upwelling centers such as at Pt. Año Nuevo to the north of Monterey Bay. The upwelling jet has an offshore component and a southward component. In the case of the upwelling front that forms inshore of the southward upwelling jet, a region with reduced winds and high intensity heating from the Sun is called an *upwelling shadow* or *retention zone* (Graham et al., 1992; Graham and Largier, 1997). Within open embayments such as Monterey Bay, the upwelling jet cuts the bay off from the ocean coast and intense warming leads to strong nearshore stratification.

1.1.4 Biogeochemistry

Although low dissolved oxygen (DO), acidic waters occur naturally throughout the global ocean (Bograd et al., 2008; Deutsch et al., 2011; Hofmann et al., 2011; Booth et al., 2012), anthropogenic emissions continue to exacerbate natural variations in DO and acidification (Diaz and Rosenberg, 2008; Doney, 2010). CO₂ also acts directly on the ocean by decreasing seawater pH and consequently the aragonite saturation state (Ω_{ar}), and indirectly to reduce DO (Feely et al., 2018). Due to climate change, expansion of Oxygen Minimum Zones (OMZ) is expected as temperature increases and the oceanic thermocline shoals. Thermocline shoaling is especially important for regions with intense wind-driven upwelling such as the California Current Large Marine Ecosystem (CCLME) which is analogous to the California Current System identified above (McClatchie et al., 2010; Deutsch et al., 2011). Wind-driven upwelling brings deep low pH, low DO waters onto the continental shelf. Through other processes, such as breaking internal tides, these corrosive, hypoxic waters can enter nearshore ecosystems where biological activity can further affect DO and pH variation. Therefore, exposure of nearshore ecosystems to climate change impacts is not simply a straightforward projection from large-scale climate models. In order to understand how exposure of nearshore ecosystems to climate stressors may change in the future, we need to understand how all of these factors interact.

Ocean CO₂ uptake has led to a pH decline of 0.1 units over the last 250 years (Gruber et al., 2012) and an oxygen decline between 0.002 and 0.01 mg L⁻¹ (Stramma et al., 2008) and will have a continued decrease in pH and oxygen of over 70% and approximately 13%

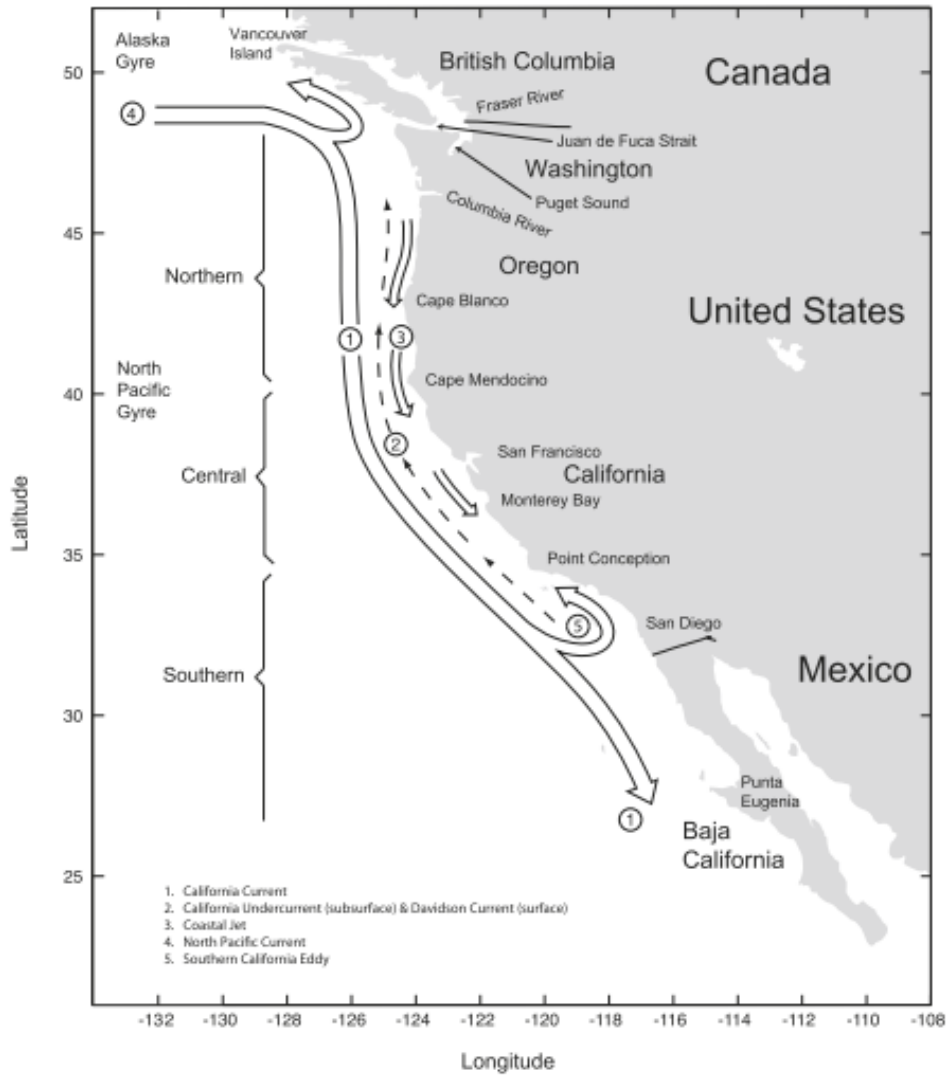


Figure 1.2: Subdivision of California Current system (CCS) and its major processes. From Checkley and Barth (2009).

respectively for some regions of the North Pacific in future scenarios (Bopp et al., 2013; Kwiatkowski and Orr, 2018). At depth, the CCLME already has a natural decrease in both pH and DO with a variation of 4 fold in the first 100 meters (Feely et al., 2018), and low pH waters occasionally reach the surface during upwelling season (Chan et al., 2017). In the nearshore, short term fluctuations can reach 0.5 units for pH and 12.5 mg/L for oxygen in a ~ 12.42 hour cycle (M2 tide) is observed in Monterey Bay, CA, likely due to a combination of tidal and wind forcing (Booth et al., 2012).

Ocean acidification and hypoxic zones are intimately linked especially Eastern Boundary upwelling systems (EBUSs). Regions of low Oxygen are found where thermal stratification and high rates of respiration occur (Gobler and Baumann, 2016) and therefore are found at all oceans in different depths. The Pacific ocean accounts for a major volume of low O_2 waters and are expected to further deoxygenate in the future (Deutsch et al., 2011; Hofmann et al., 2011; Bopp et al., 2013). The major portion of low DO waters found in the Eastern Boundary region of the Pacific is a consequence of the interaction between lack of ventilation in the thermocline and oxygen consumption in regions of high productivity, for example, upwelling regions (Karstensen et al., 2008). A direct seasonal relationship exists between a decline in oxygen concentrations and shoaling of denser isopycnals due to alongshore equatorward winds (upwelling) on the west coast of the US (McClatchie et al., 2010; Chan et al., 2017; Feely et al., 2018). The volume of low oxygen waters are expected to expand due to warming (Deutsch et al., 2011; Bopp et al., 2013). In the nearshore, nonlinear internal waves also play an important role by bringing low oxygen, low pH waters into coastal ecosystems (Walter et al., 2014; Woodson, 2018).

An important consequence for a decline in pH is the availability of carbonate ions in the water which are important for formation of shells in calcifiers. Calcifiers extract CO_3^{2-} from seawater to create $CaCO_3$. Extraction of CO_3^{2-} is affected by the aragonite saturation state Ω_{ar} , defined as the ratio of the product of Ca^{2+} and CO_3^{2-} by the apparent solubility product (K'_{sp}). The solubility constant is directly related to Dissolved Inorganic Carbon (DIC) and Alkalinity in seawater (Doney et al., 2009). Corrosive water occurs when Ω_{ar} is < 1.0 which decreases calcification rates due to a decline of carbonate ion concentrations (CO_3^{2-}) (Orr et al., 2005). In the CCLME, events with undersaturated Ω_{ar} are expected

to happen over 50% of the time in the future compared to present conditions (Chan et al., 2017). Meanwhile, low Ω_{ar} brought by upwelled waters is already reported in Monterey Bay, CA (Koweek et al., 2017).

Marine ecosystems are acclimated to particular conditions, and therefore, fluctuations of oxygen, pH and temperature can cause stress on organisms. For example, kelp forest biomass is replaced by turfs in high CO₂ and high temperatures in laboratory (Connell and Russell, 2010). In addition, the red abalone, *Haliotis rufescens* experiences reduced fertilization when exposed to hypoxia and ocean acidification conditions (Boch et al., 2017). Calcifying organisms are expected to have their shells dissolved as well as experience growth inhibition in undersaturated aragonite waters (Orr et al., 2005; von Dassow et al., 2018). Yet, these are only single stressor effects. The effects of multiple stressors with high frequency variability (diurnal or higher) on organisms are just beginning to be investigated. For example, larval bivalves show a decreased survival and growth when exposed to diurnal fluctuations of ocean acidification and hypoxia conditions (Gobler et al., 2017). As above, *H. rufescens* shows a decline in fertilization in response to pH and oxygen levels associated with climate change with a distinct threshold around pH of 7.6 (Boch et al., 2017). Interestingly, warm temperatures appear to have a mediating effect on the fertilization response (Boch et al., 2017).

The understanding of how pH, DO, and temperature vary over diurnal and semi-diurnal periods in a region of upwelling and if this variability causes stress on the local biota is still not well understood (Frieder et al., 2014; Boch et al., 2017; Chan et al., 2017; Feely et al., 2018; Woodson, 2018). My thesis aims to understand how multiple co-varying stressors (pH, T, DO) in coastal regions may change from present to predicted future conditions (increasing levels of CO₂) and how these scenarios affect exposure of nearshore organisms to stressful conditions.

1.2 Goals

This study is divided in two sections. In Chapter 2, I develop and calibrate an idealized model using *in situ* data during the upwelling period in the region of Monterey Bay. Also in Chapter 2, I examine different scenarios of climate change for the year 2100 using the model. As a result, I model the variability of O_2 , pCO_2 and pH in a nearshore region affected by upwelling, winds, and tides. My first hypothesis is that daily variability of pH, DO, and temperature during the upwelling season are going to be stronger in the future. The second hypothesis is that, climate change scenarios will increase the exposure of organisms to low oxygen, low pH waters due the intensification of hypoxia and increased acidification in upwelling regions.

Chapter 2

FORECASTING EXPOSURE OF NEARSHORE ECOSYSTEMS TO CLIMATE CHANGE IMPACTS¹

¹Fagundes, M. and Woodson, C.B. To be submitted to Biogeosciences.

Abstract

Climate change is expected to increase temperature, and decrease oxygen and pH. Locally, the effects of these high temperature, low oxygen and low pH waters and how they affect the local biota are still not well understood. Some studies have demonstrated that daily exposure shows different results than time varying temperature, pH, and DO. However for climate predictions, coarse temporal and spatial resolution model outputs are used at global scales that cannot replicate the high variability in the nearshore. This study uses a coupled ocean circulation (ROMS) and biogeochemical model applied to the nearshore environment of Monterey Bay for present and future IPCC scenarios. I use the model to estimate daily exposure for two benthic organisms based on time-varying variables for future scenarios. The results show increasing exposure for different RCP scenarios for both species as well as a bias in results when applying large scale model values. My results demonstrate that the idealized model can be applied to forecast future conditions for nearshore ecosystems that can inform laboratory experiments.

2.1 Introduction

Low dissolved oxygen (DO), acidic waters occur naturally throughout the global ocean (Bograd et al., 2008; Deutsch et al., 2011; Hofmann et al., 2011; Booth et al., 2012) and anthropogenic emissions are acting to further reduce both oxygen content and pH of oceanic waters (Diaz and Rosenberg, 2008; Doney, 2010). CO_2 also acts directly on the ocean by decreasing seawater pH and consequently the aragonite saturation state (Ω_{ar}) and indirectly by reducing oxygen solubility in seawater (Feely et al., 2018). Due to climate change, expansion of Oxygen Minimum Zones (OMZ) is expected as temperature increases and thermocline shoals. Expansion of OMZs is particularly important in regions characterized by strong wind-driven upwelling such as the California Current Large Marine Ecosystem (CCLME) (McClatchie et al., 2010; Deutsch et al., 2011). Upwelling brings waters that are naturally low in DO and pH onto the continental shelf, where through other exchange processes, these waters can even enter nearshore ecosystems where biological activity can further alter DO and pH. In these shallow environments, exposure to low oxygen, low pH waters is also affected by tides and winds. Consequently, understanding how nearshore ecosystems will respond to future climate change is not as straightforward as direct down-scaling of large-scale climate model projections. In order to understand how exposure of nearshore ecosystems to climate stressors may change in the future, we need to understand how all of these factors interact.

An important consequence for a decline in pH is the availability of carbonate ions in the water which are important for formation of shells in calcifiers. Another important variable for CaCO_3 formation is the aragonite saturation state (Ω_{ar}), defined as the ratio of the product of Ca^{2+} and CO_3^{2-} by the apparent solubility product (K'_{sp}) which is linked to Dissolved Inorganic Carbon (DIC) and Alkalinity in seawater (Doney et al., 2009). Thus, corrosive water occurs when Ω_{ar} is < 1.0 which decreases calcification rates due to a decline of carbonate ion concentrations (CO_3^{2-}) (Orr et al., 2005).

Acidic waters with hypoxic conditions when acting together have demonstrated negative effects on some larval invertebrates (Gobler et al., 2014). However, not all organisms have the same lethal threshold for oxygen (Vaquer-Sunyer and Duarte, 2008). For example, fish exhibit a lethal threshold of approximately 1.54 mg/L (Vaquer-Sunyer and Duarte, 2008).

Demersal fish and benthic organisms can also have the effect of low oxygen enhanced by respiration causing death in upwelling regions (Graham, 2004). Furthermore, invertebrates mortality has been suggested due to waters with oxygen concentration below 4.6 mg/L in Mexico (Micheli et al., 2012).

Regions of low oxygen and low pH are found in all oceans at different depths where thermal stratification and high rates of respiration occur (Gobler and Baumann, 2016). The Pacific ocean accounts for a major volume of low O₂ waters and these waters are expected to further deoxygenate in the future (Deutsch et al., 2011; Hofmann et al., 2011; Bopp et al., 2013). In regions such as Eastern Boundary upwelling systems (EBUs), deoxygenation is also critically linked with ocean acidification. The major portion of low DO, low pH waters found in the Eastern Boundary region of the Pacific is a consequence of the interaction between lack of ventilation in the thermocline and oxygen consumption in regions of high productivity, for example, upwelling regions (Karstensen et al., 2008). Ocean CO₂ uptake has led to a pH decline of 0.1 units over the last 250 years (Gruber et al., 2012) and an O₂ decline of 0.9 mg L⁻¹ in the past 15 years (Ren et al., 2018) and will further decrease pH and O_{2sat} by over 70% and 13% respectively in some regions of the North Pacific in future scenarios (Cabr e et al., 2015; Kwiatkowski and Orr, 2018). At depth, the CCLME already has a natural decrease in pH and DO with a variation of 4-fold in the first 100 meters (Feely et al., 2018), and low pH waters occasionally reach the surface during upwelling season (Chan et al., 2017). Also, a direct seasonal relationship exists between a decline in oxygen concentrations and shoaling of denser isopycnals due to alongshore equatorward winds on the west coast of the US (McClatchie et al., 2010; Chan et al., 2017; Feely et al., 2018), and are expected to intensify the volume of low oxygen due to warming (Deutsch et al., 2011; Bopp et al., 2013). Locally, other processes also affect the transport of low oxygen waters as well as acidic waters into the nearshore environments. Short term variability fluctuations in pH and DO that reach 0.5 units and 4 mgL⁻¹ respectively at the surface in a \approx 13 hour cycle (M2 tide) is observed in Monterey Bay, CA, likely due to tidal and wind forcing (Booth et al., 2012). Nonlinear internal waves also play an important role by bringing low oxygen, low pH waters into coastal ecosystems (Walter et al., 2014; Woodson, 2018), and consequently affecting the local biota.

Marine ecosystems and the organisms that comprise them are acclimated to particular conditions, and therefore, deviations of oxygen, pH and temperature from natural background conditions can cause stress on organisms. For example, kelp forest biomass is replaced by turfs in high CO₂ and high temperatures in laboratory (Connell and Russell, 2010). In addition, the abalone, *Haliotis rufrescens* experiences reduced fertilization when exposed to hypoxia and ocean acidification conditions (Boch et al., 2017). Calcifying organisms are expected to have their shells dissolved as well as experience growth inhibition in undersaturated aragonite waters (Orr et al., 2005; von Dassow et al., 2018). Yet, these are only single stressor effects. The effects of multiple stressors on organisms for diurnally-fluctuating low pH and low DO conditions on organisms are just beginning to be investigated. For example, larval bivalves show a decreased survival and growth when exposed to diurnal fluctuations of ocean acidification and hypoxia conditions (Gobler et al., 2017). Similarly, *H. rufrescens* shows a decline in fertilization in response to climate change pH and oxygen (Boch et al., 2017).

Understanding how pH, DO, and temperature varies over diurnal and semi-diurnal periods and if this variability causes stress on the local biota is still not well understood (Frieder et al., 2014; Boch et al., 2017; Chan et al., 2017; Feely et al., 2018; Woodson, 2018). This study aims to understand how variability in multiple co-varying stressors (pH, T, DO) may change from present to predicted future conditions (increasing levels of CO₂) and how these scenarios affect exposure of nearshore organisms to stressful conditions. My goal is to develop and calibrate an idealized model using *in situ* data during the upwelling period in the region of southern Monterey Bay near Hopkins Marine Station (Figure 2.1). I will then run different scenarios of climate change for the year 2100 using the model. This paper is organized as follows: Section 2 gives a description of the study site and set up of the numerical model used. Section 3 provides the data and analysis applied. Section 4 compares the model with *in situ* data and quantifies climate scenarios. Section 5 presents discussion for the previous section. Finally, conclusions are presented in section 6.

2.2 Monterey Bay configuration

2.2.1 Study Site

Monterey Bay is the largest bay on the California coast, and has a total area of approximately 1481 km² (Figure 2.1). Monterey Bay is considered rich biologically and ecologically because of the kelp forest region and it generally consists of kelp forests out to 15 m depth (Koweeck et al., 2017). Due to its high primary production and capacity to regulate pH (Miller et al., 2011; Reed et al., 2011; Krause-Jensen et al., 2016), the giant kelp in California sustains over 200 different species from phytoplankton to mammals creating a dynamic and productive environment (Graham, 2004).

During spring and early summer temperatures are the coolest (Tseng et al., 2005). During this period, salinity is approximately 34, temperature ranges from 9-13 °C at 17 m depth (Booth et al., 2012), DO varies from as low as 100 $\mu\text{mol kg}^{-1}$ (3.2 mg/L for T=13°C, S=34 at 17 m) to as high as 300 $\mu\text{mol kg}^{-1}$ (9.62 mg/L for T=13 °C, S=34 at 17 m), and pH varies from 7.7 to 8.1 (Feely et al., 2018).

Seasonal equatorward winds blow during spring and summer over the California coast causing offshore Ekman transport (Huyer, 1983). During the same months, filaments of water originate from Point Año Nuevo to the north are trapped within the Bay, where they warm due to solar radiation forming lens of warm water close to shore (Breaker and Broenkow, 1994; Rosenfeld et al., 1994). Furthermore, a weak cyclonic eddy is observed within the bay due to the coastal geometry (Breaker and Broenkow, 1994; Tseng et al., 2005). Inside the bay, sea breezes and tides drive semi-diurnal and diurnal upwelling frequency signal (Woodson et al., 2007; Woodson, 2013).

The main three barotropic tide constituents in the region are M2, K1, and S2 that are responsible for over 80% of the total amplitude observed (Carter, 2010). In the southern region of the bay, tides are mainly responsible for the cross-shelf velocity (Woodson, 2013), where the interaction of these surface tidal currents with the steep topography create internal waves (internal tides) at tidal frequencies (Garrett, 2003; Dettner et al., 2013). These internal tides have speed on the order of 0.05-0.2 m/s (Walter et al., 2014). The instability of these

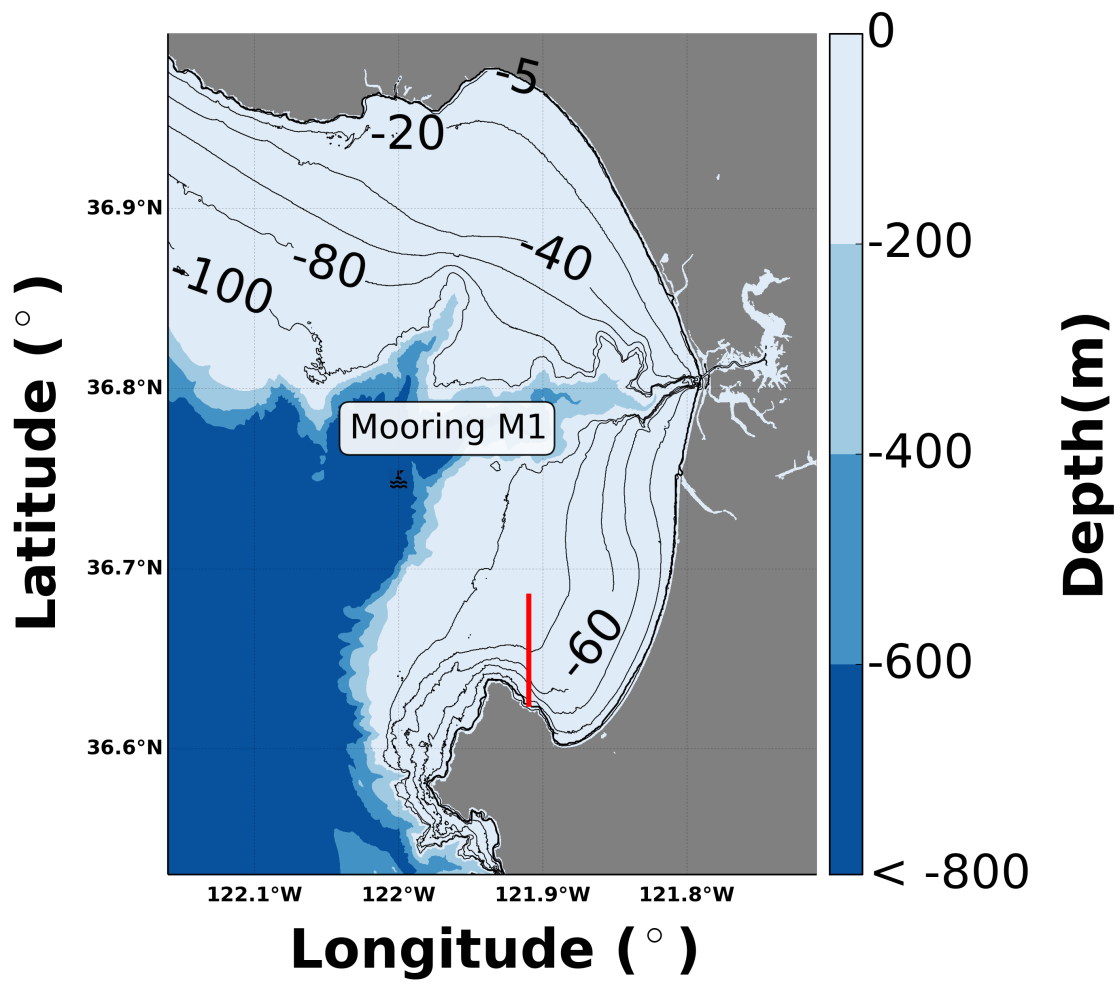


Figure 2.1: Model domain based on the cross shore section (red line).

internal waves and consequent breaking leads to the formation of an internal bore that moves upslope and brings cold, low DO, low pH waters into nearshore kelp forest ecosystems (Martini et al., 2012). Kelp forests, then, trap this fluid creating an internal tide pools (Leary et al., 2017). Internal tide pools are regions with characteristics of deep, low oxygenated, and acidic waters that have a longer residence time and cause harm to organisms (Leary et al., 2017).

2.2.2 Model Description

The model used in this experiment is the Regional Ocean Modelling System (ROMS) (Haidvogel et al., 2008). The model domain was created based on the Monterey Bay continental shelf described in Walter et al. (2014) with a maximum offshore depth of approximately 80 m (Figure 2.2). The initial settings for the model are described in Table 2.3. The model has a critical depth $h_c = 20$ m, a bottom stretching factor of $\theta_b=4.0$, and a surface stretching factor of $\theta_s = 6.5$. The boundary conditions used for the physics and the biological tracers are described in Tables 2.1 and 2.2. The period for the theoretical runs is from 1 May 2013 to 30 July 2013. This period is considered a typical spring upwelling season for the region of Monterey Bay (Woodson et al., 2007).

The biogeochemical model used is described in Fennel et al. (2006, 2008). I use the non-conservative option where alkalinity affects air-sea CO_2 fluxes. Carbon dioxide partial pressure ($p\text{CO}_2$) is computed only in the first layer of the domain. Moreover, Total alkalinity (TA) and Dissolved inorganic carbon (DIC) are diffused and advected as tracers for the model. Local alterations (i.e: primary productivity and respiratory processes) for DIC are calculated based on Redfield ratio Fennel et al. (2008). Oxygen dynamics are also added in order to compute fluctuations in dissolved oxygen content or hypoxia development.

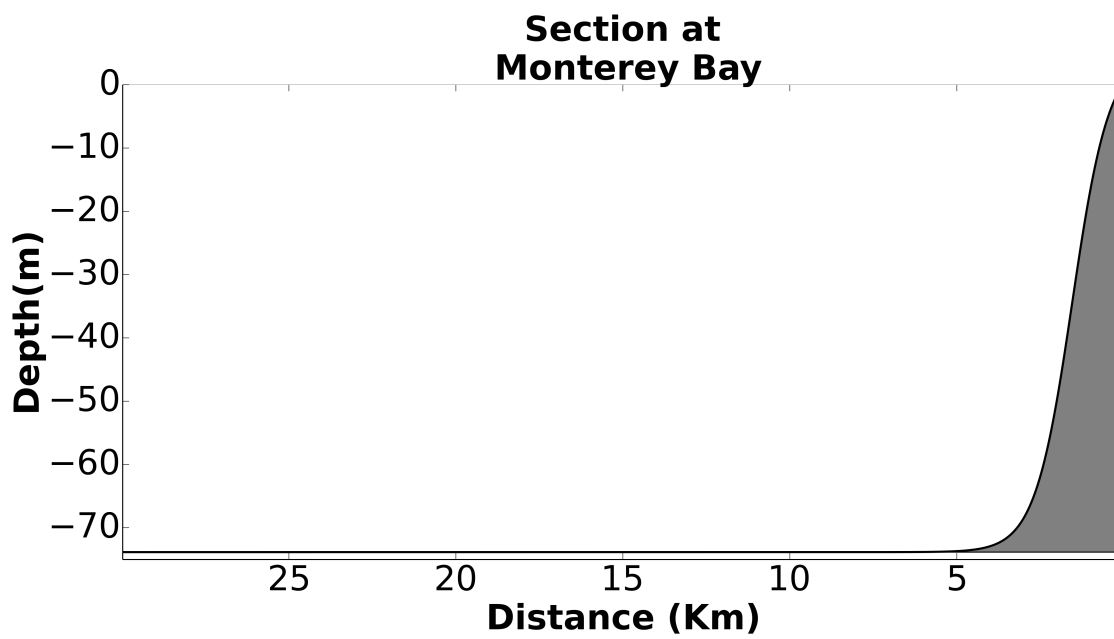


Figure 2.2: Vertical view of the domain based on Walter et al. (2014).

Table 2.1: Boundary Conditions for the domain.

	East	West	North	South
Free Surface	Per	Per	Cha	Clo
2D U-momentum	Per	Per	Cla	Clo
2D V-momentum	Per	Per	Fla	Clo
3D U-momentum	Per	Per	Rad	Clo
3D V-momentum	Per	Per	Cla	Clo
Mixing TKE	Per	Per	RadNud	Clo
Temperature	Per	Per	RadNud	Clo
Salinity	Per	Per	RadNud	Clo

* Per = Periodic; RadNud = Radiation-Nudging; Fla = Flather (2D momentum);
Clo = Closed; Cha = Chapman; Cla = Clamped.

Table 2.2: Boundary Conditions for the Biological tracers.

	East	West	North	South
NO3	Per	Per	RadNud	Clo
NH4	Per	Per	RadNud	Clo
Chlorophyll	Per	Per	RadNud	Clo
Phytoplankton	Per	Per	RadNud	Clo
Zooplankton	Per	Per	Clo	Clo
LdetritusN	Per	Per	Clo	Clo
SdetritusN	Per	Per	Clo	Clo
LdetritusC	Per	Per	Clo	Clo
SdetritusC	Per	Per	Clo	Clo
TIC	Per	Per	RadNud	Clo
Alkalinity	Per	Per	RadNud	Clo
Oxygen	Per	Per	RadNud	Clo

* Per = Periodic; RadNud = Radiation-Nudging; Clo = Closed.

L = large, S = small.

Table 2.3: Initial settings for the Idealized case.

Model Setup	
Resolution	50 x 200 m
Dt	30 s
Sigma Layers	50
Atmospheric Forcings	winds, radiation
Period of Integration	3 months
Output	Hourly
Oceanic Forcings *	M2 =0.062 m/s, K1=0.055 m/s

* Ocean Forcing estimated from cross-shore barotropic currents at M1 near model offshore boundary.

2.3 Data

2.3.1 Atmospheric Forcing

For this idealized experiment, I considered sea breeze winds. The sea breeze in Monterey Bay is linked to large-scale weather patterns that also drive region-scale upwelling. During strong upwelling periods, the diurnal sea breeze is present. However during relaxation of upwelling winds, the diurnal sea breeze does not develop. The upwelling-relaxation cycle in this region is approximately 7 days of upwelling followed by 3 days of relaxation (10 day cycle). Sea breeze winds were used in order to simulate the movement of warm lenses. Winds were ramped in the first 20 days of simulation to insure model stability and both used the same equation to peak during the same periods. The equation 2.1 is shown below:

$$winds = A \sin(Period_{10d} time) + B$$

For $winds > 0$:

$$\frac{winds(winds > 0)}{2} \sin\left(\frac{-3\pi}{4} + Period_{24h} time(winds > 0)\right) + \frac{winds(winds > 0)}{2} \quad (2.1)$$

$$winds = \begin{cases} if < 0 & winds = 0 \\ if > 0 & winds = fraction * winds \end{cases}$$

Where, A=4, and B=2 are the coefficients used to create the time series. $Period_{24h} = \frac{2\pi}{3600s \times 24h}$ and $Period_{10d} = \frac{2\pi}{10d \times 24h \times 3600s}$, fraction value was $\frac{3}{5}$ for the sea breeze. Thus, negative winds for both situations were considered zero (Figure 2.3).

Shortwave radiation (swr) was imposed hourly using a sinusoidal function with varying amplitude depending on the scenarios. The following values were used 150 W/m², 150 W/m², 260 W/m², 260 W/m², and 300 W/m² for present, RCP26, RCP45, RCP60, and RCP85, respectively. These values were chosen to prevent the model from losing heat over the period of each run and are all significantly lower than observed values for present day of 600-800 W/m² during summer. An example of the shape of the shortwave impose is shown in Figure

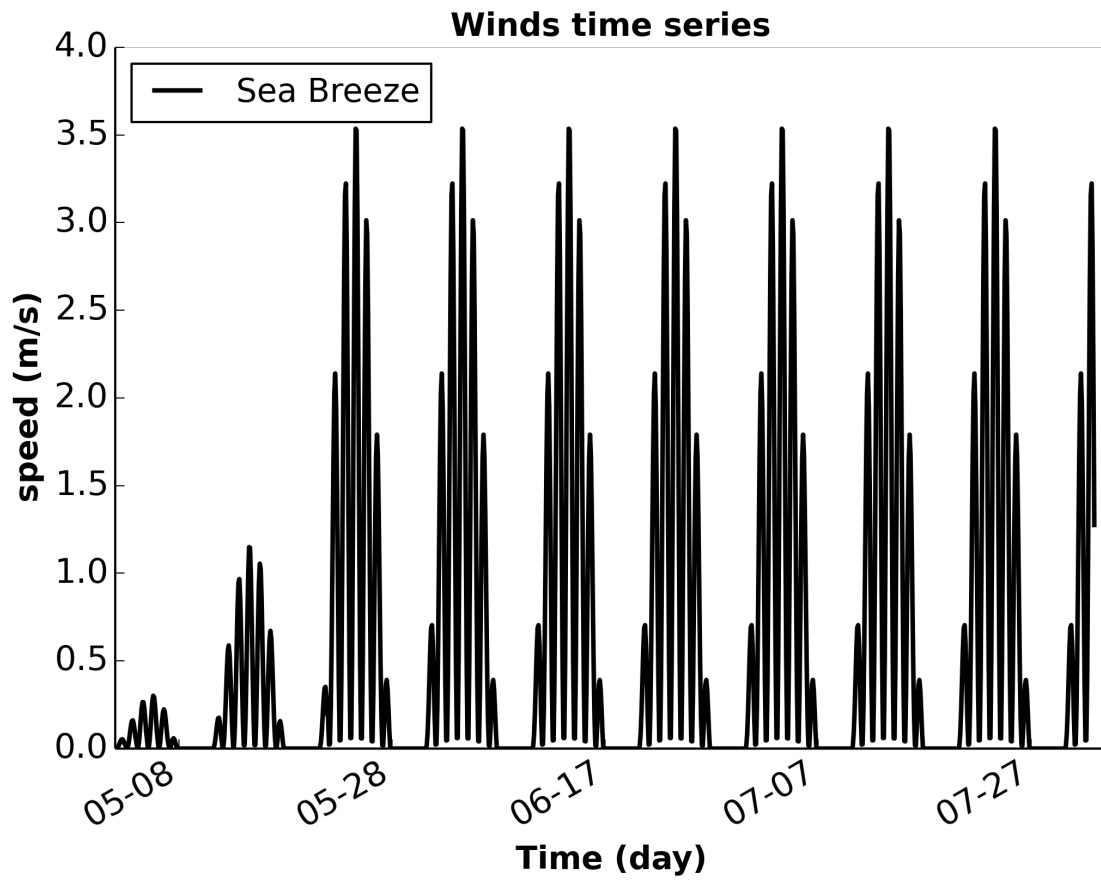


Figure 2.3: Sea breeze and downwelling winds time series used for the simulation.

2.4. Air temperature values used were constants and were 1°C higher than the maximum surface temperature in the model for each scenario. Air Pressure used was 1013.25 mb for all scenarios and also constant. Other atmospheric forcings such as, longwave radiation, rain, cloud were considered zero for the entire experiment since they do not play an important role during this period.

2.3.2 Ocean Forcing

The model is initialized from rest (all velocities = 0). I represent the tidal cycle by forcing the model at the northern boundary using a meridional component of velocity with a hourly frequency that is created using equation 2.2:

$$vel(z, t) = \begin{cases} 0, & \text{if } z \geq D_{pycnocline}. \\ M_2 \cos(Mt - 1.3\pi) + K_1 \cos(Kt + 1.3\pi) & \text{otherwise.} \end{cases} \quad (2.2)$$

in order to initiate the model, the four first hours were set to zero and M_2 and K_1 velocities were set to 0.062 m/s, 0.055 m/s, respectively. $M = 2\pi / (12.42\text{hr} * 3600)$ and $K = 2\pi / (23.93\text{hr} * 3600)$ are the tidal frequencies (Figure 2.5). Due to the fact, the model is 2D and therefore does not represent well the background circulation that happens in the Southern region of the Monterey Bay (Suanda et al., 2011), the velocity is set to zero from surface to the pycnocline depth (Figure 2.6). The thicker arrows in Figure 2.6 indicate subtidal currents, the dashed line is the limit of my domain, and the smaller arrows indicate the velocity profile observed with *in situ* data (not shown) nearshore. Also, warm waters in the diagram indicate the region of lenses formed during spring and summer seasons (Tseng et al., 2005; Carter, 2010). These lenses work as a barrier for the tidal currents when these try to push cold and well mixed waters towards nearshore.

2.3.3 Initial and Boundary conditions

For our simulations I considered a homogeneous salinity ($S=34$) for the entire domain since the variation is less than 0.4 over an entire year and less than 0.05 during the upwelling season (Kowek et al., 2017). The initial and boundary stratification is then controlled

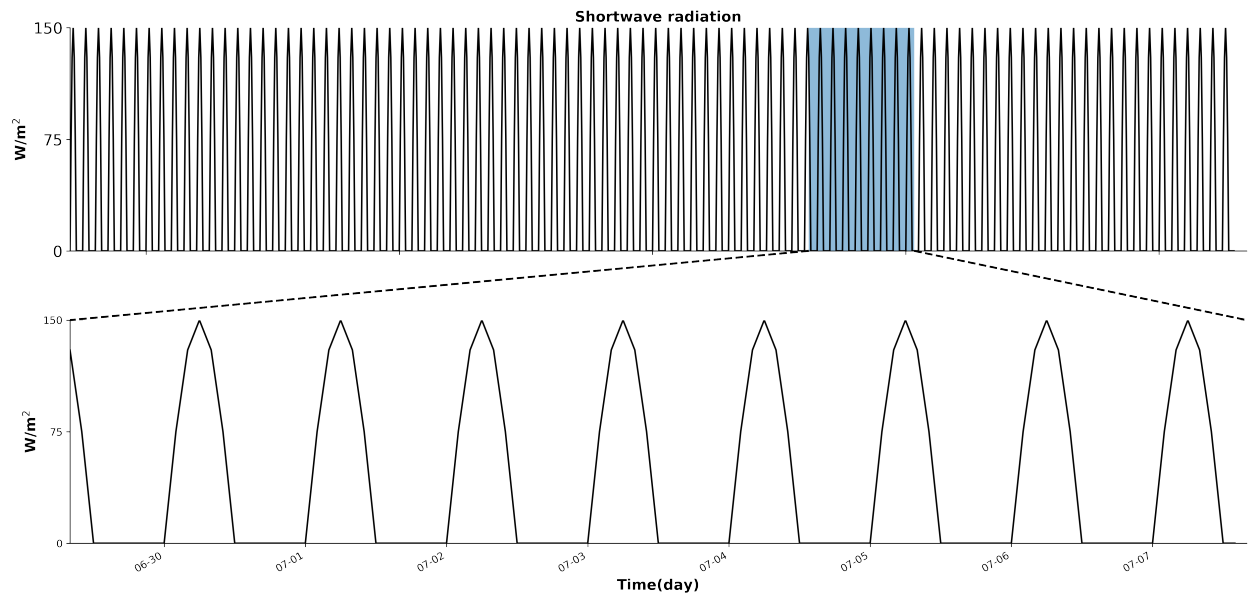


Figure 2.4: Time series used for shortwave radiation.

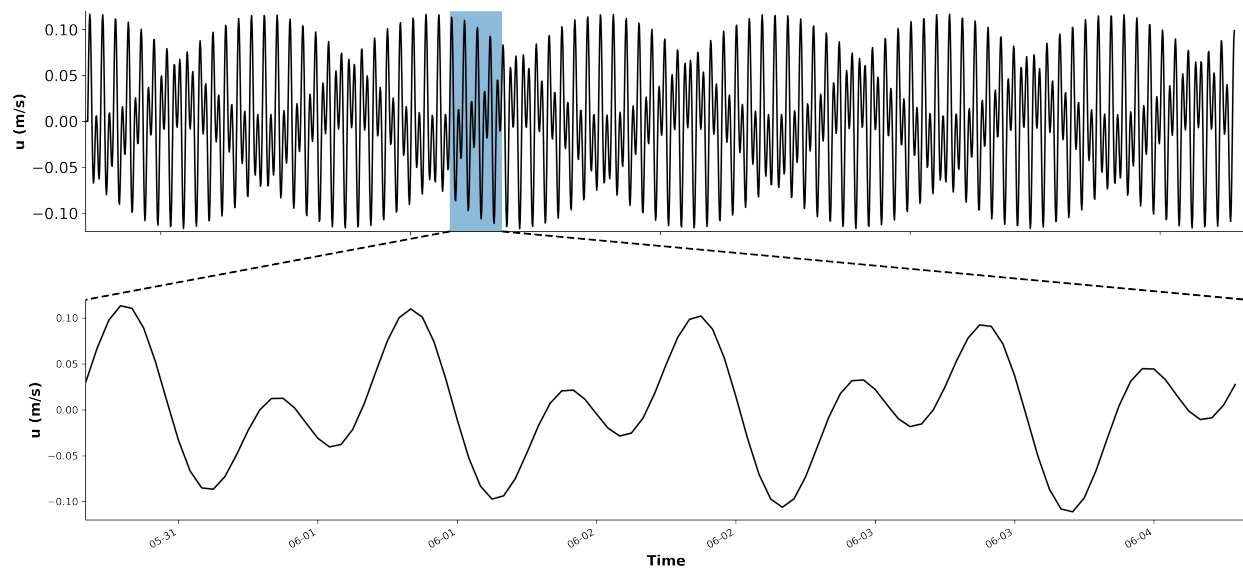


Figure 2.5: Time Series of velocity used to force West boundary in the model.

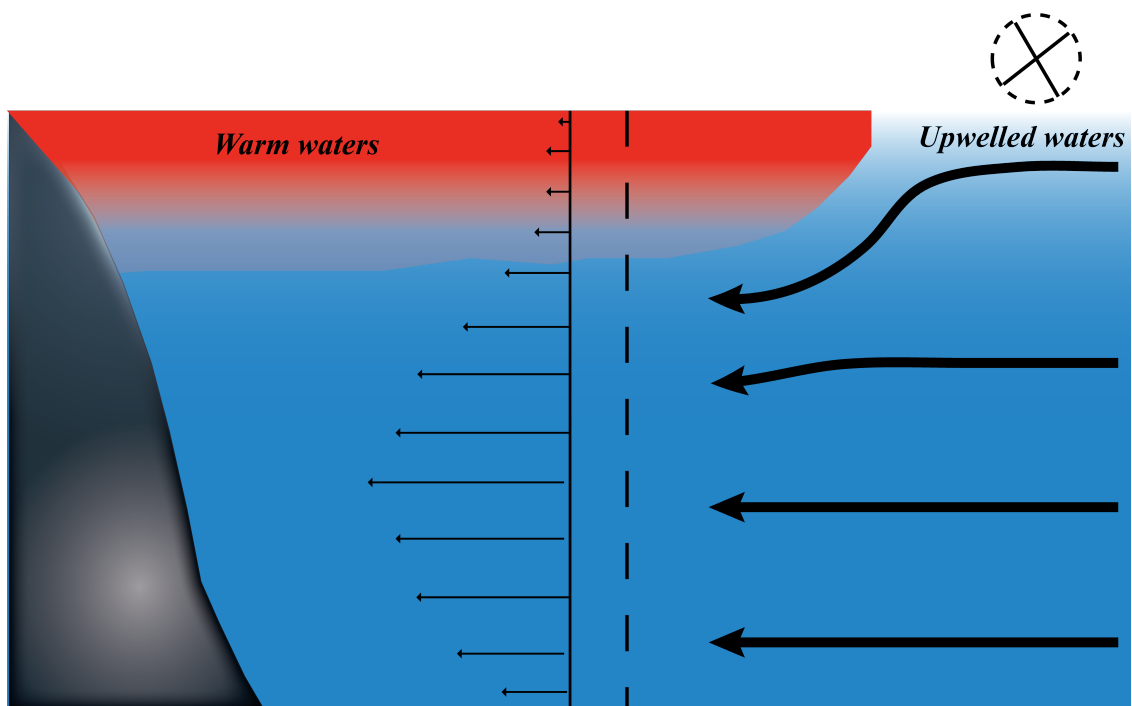


Figure 2.6: Schematic of tidal currents subduction and vertical velocity profile at the site of study.

by temperature profile. I represent the initial conditions of the other variables such as temperature, total alkalinity (Talk), dissolved inorganic carbon (DIC), dissolved oxygen (DO), and nitrogen (N) with an analytical form:

$$var(z) = \begin{cases} \Delta var * D_{pycnocline}^\alpha & \text{if } z \geq D_{pycnocline} \\ \Delta var * z^\alpha & \text{otherwise} \end{cases} \quad (2.3)$$

where var is each variable identified above, z is the depth, α is a fit coefficient for each variable determined from observational data. An environment with initially no detritus was considered for this idealized case. The data used for the initial and boundary conditions of phytoplankton and chlorophyll profiles were taken from Schuckmann et al. (2016). A reasonable zooplankton concentration was imposed as an initial condition to keep the domain biologically stable.

2.3.4 CO2SYS

I calculated pH and Ω_{ar} using CO2SYS (Lewis and Wallace, 1998) package in MATLAB at the closest grid point to 15 m depth using temperature, salinity, DIC, and TA calculated from the simulations. I assumed concentrations of phosphate and silica based on Koweek et al. (2017). I used dissociation constants for H_2CO_3 and HCO_3^- by Dickson and Millero (1987), and hydrogen sulfate ion constant (HSO_4^-) from Dickson (1990).

2.3.5 Present and Future data

Surface and bottom values for present scenario were based on Koweek et al. (2017). The mean of the 3 upwelling month (May, June, July) surface values of DIC and oxygen from Representative Concentration Pathway (RCP) scenarios 2.6, 4.5, 6.0, and 8.5 for the year of 2100 were taken from the 4th report of the IPCC (2013). For the scenarios 4.5 and 6.0, I calculated the ratio between for both RCP2.6 or RCP8.5 and present at the surface and at the bottom. Subsequently I calculated the ratio between the surface ratio and bottom ratio for both scenarios and found a linear relation between surface and bottom with a slope

equal to 0.14 in both scenarios calculated. Thus, I applied the same ratio to find the bottom values for the other two scenarios. DIC for RCP8.5 was extrapolated from surface value and compared with published data Resplandy et al. (2013) which shows good agreement between pH. The same procedure used to calculate DO was applied for RCP 2.6, 4.5 and 6.0 scenarios. In order to confirm that the ratio was corrected I compared pH for RCP2.6 and Resplandy et al. (2013) and I found a difference of 0.01 between both. Therefore, I applied to the other two scenarios (Table 2.4). The RCP4.5 pH has a value pretty similar to RCP2.6 and RCP6.0 pH has a pH similar to RCP8.5 pH. These values might represent the thresholds for a transition between close to present scenarios and extreme scenarios. The surface and bottom TA values are the same used for present condition.

Equation 2.3 was then applied in order to find profiles used for the simulations. Thus, parameters for the equation were found applying $z=10$ meters and results found and showed in the table 2.4. The initial and boundary stratification is then determined by equation 2.3 with $z=10$ meters, and using table 2.4 in order to calculate α and $D_{pycnocline}$. The initial and boundary profiles for present and future scenarios are shown in Figure 2.7. PH profile was calculated using CO2SYS.

All the oxygen profiles were shifted 60 mmol m^{-3} (1.87 mg L^{-1} for $T=13^\circ\text{C}$ and $S=34$). This was done in order to simulate high primary production due to kelp forests (Reed et al., 2011) that is not added to the model. Surface waters in southern Monterey are commonly super-saturated in oxygen due to production by kelp forests. Thus, values for oxygen at depth increased between 45 and 65 mmol m^{-3} (1.40 and 2.03 mg L^{-1} for $T=8^\circ\text{C}$ and $S=34$). Overall, temperature at the bottom kept the same with exception to RCP60 that increased 0.2°C (see table 2.5).

Table 2.4: Values for present and future scenarios at surface and bottom used to fit the equation and used as Boundary condition for the Idealized experiment.

Scenarios	Location	T (°C)	pCO_{2atm} (ppm)	O_2 (mmol m ⁻³)	O_2 (mg L ⁻¹)	TA(mEqm ⁻³)	DIC(mmolC m ⁻³)	pH	Ω_{ar}
Present	Surface	13	400	300	9.38	2300	2073	8.11	2.5
	Bottom	8		30	0.94	2305	2280	7.63	0.77
RCP 2.6	Surface	16.20	430	243.7	7.61	2300	2057	8.01	2.35
	Bottom	10.27		25	0.78	2305	2300	7.56	0.75
RCP 4.5	Surface	16.95	540	241.7	7.55	2300	2103	7.97	1.94
	Bottom	10.35		22.9	0.72	2305	2318.3	7.51	0.65
RCP 6.0	Surface	17	670	236.7	7.40	2300	2154	7.85	1.75
	Bottom	10.21		18.6	0.58	2305	2383.3	7.28	0.38
RCP 8.5	Surface	19	930	232.8	7.28	2300	2167	7.79	1.37
	Bottom	10.81		15	0.47	2305	2400	7.26	0.3

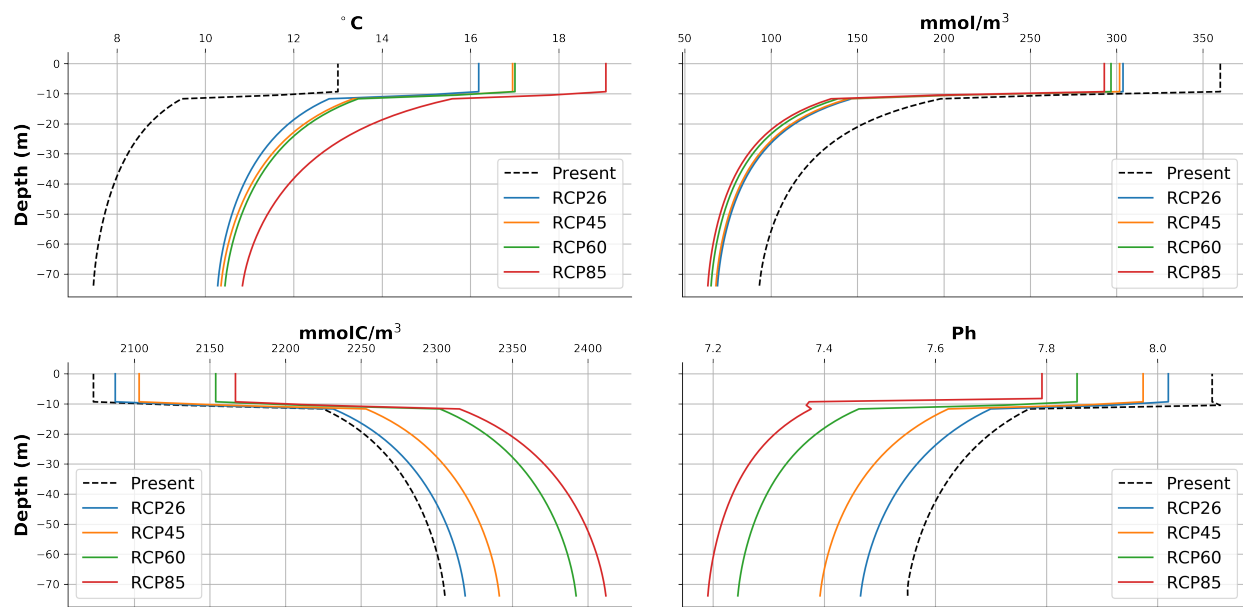


Figure 2.7: Initial and Boundary Conditions profiles for present and future scenarios: a) Temperature, b) O_2 , c) DIC, d) pH.

Table 2.5: Final values for present and future scenarios at bottom found by fitting the equation and used as Initial and Boundary conditions for the Idealized experiment.

Scenarios	Location	T (°C)	O ₂ (mmol m ⁻³)	O ₂ (mg L ⁻¹)
Present	Surface		360	11.25
	Bottom	8	93.24	2.91
RCP 2.6	Surface		303.7	9.50
	Bottom	10.28	69	2.16
RCP 4.5	Surface		301.7	9.43
	Bottom	10.35	68	2.13
RCP 6.0	Surface		296.7	9.27
	Bottom	10.44	65.2	2.03
RCP 8.5	Surface		292.8	9.15
	Bottom	10.83	63	1.97

2.4 Analysis

2.4.1 Spectral Analysis

In order to validate the temporal variability of the model results, power spectral analysis (using fast Fourier Transform, FFT) and the Thomson Multi-taper method is applied on a 3 week window of upwelling for temperature, pH and O_2 and compared with Booth et al. (2012) data (Figure 2.8). This method is applied since all the IC and BC are idealized values based on observations and calculated using an analytical equation. As a result, it will enable me to observe whether or not the model is capturing observed pH, DO and temperature dynamics from the Monterey Bay region.

2.4.2 Integrated exposure calculation

Exposure of organisms to stressful pH, DO, and temperature conditions is done by subtracting the raw data from the threshold value for different organisms, then setting all positive values to zero for pH and O_2 , and all negative values to zero for temperature. Next, I integrate the absolute exposure over a period of a day at 15 meters depth (eq. 2.4). Thus, the results quantify the amount each species was exposed to each stress over a period of a day similar to the degree heating day measure used to estimate thermal stress on coral reefs (Liu et al., 2014), and have been used to understand the exposure of juvenile abalone population in climate change conditions (Boch et al., 2018).

$$\phi' = \phi - \phi_{th} \begin{cases} \phi' > 0 \rightarrow \phi' = 0 & \text{for pH and } O_2 \\ \phi' < 0 \rightarrow \phi' = 0 & \text{for temperature} \end{cases} \quad (2.4)$$

$$\text{Integrated Exposure} = \int_0^t |\phi'| dt$$

Thresholds of temperature, DO, and pH are used for two species based on values found in the literature and are shown in Table 2.6. These values represent a decrease in fertilization success for red abalone (*Haliotis rufescens*) and sea urchin (*Paracentrotus lividus* and

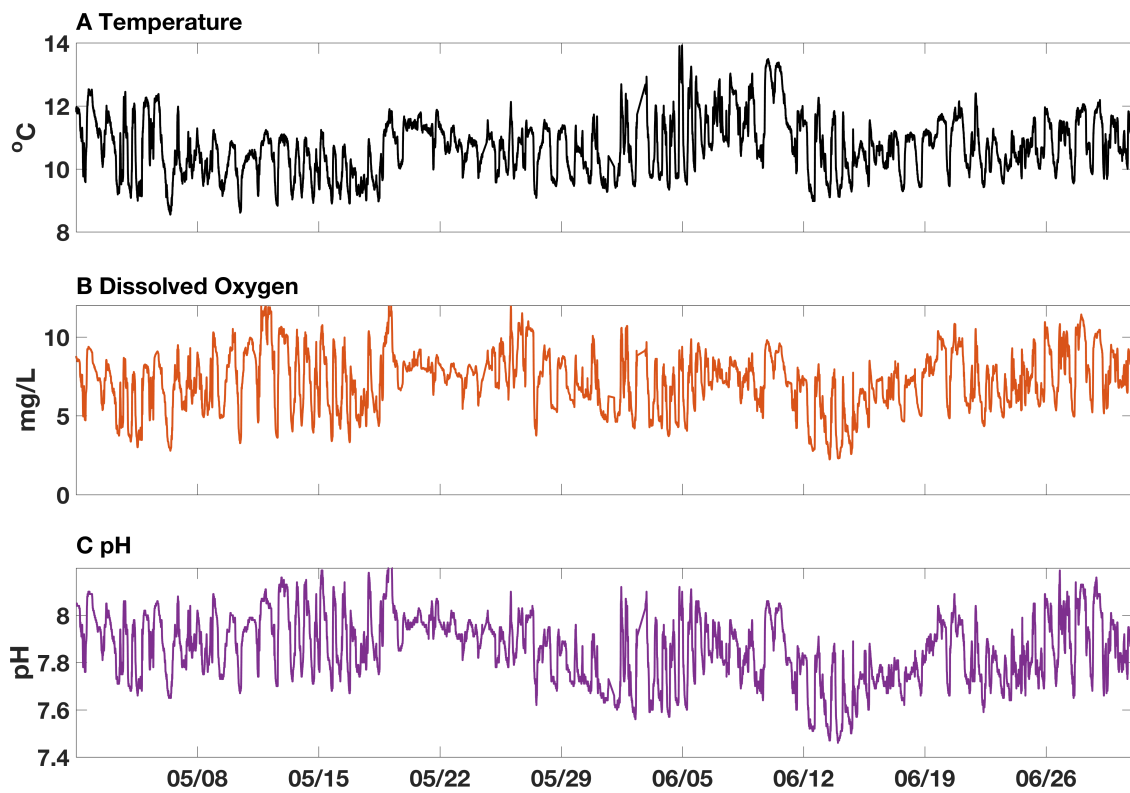


Figure 2.8: Time series of temperature, Dissolved Oxygen, and pH from Booth et al. (2012) showing for a typical period of upwelling.

Table 2.6: Threshold for fertilization and grazing success of two benthic taxa in the CCS.

Taxon	Species	Life stage	Treatments			References
			T (°C)	O ₂ (mg L ⁻¹)	pH	
gastropoda	<i>Haliotis rufescens</i>	fertilization	14	5.72	7.50	Boch et al. (2017)
echinoidea	<i>Paracentrotus lividus</i>	fertilization	15.3		7.6	Moulin et al. (2011) and Graham et al. (2016)
echinoidea	<i>Mesocentrotus franciscanus</i>	Adult		5.5		Low and Micheli (2018)

Mesocentrotus franciscanus). The values chosen had any type of negative strong effect on the populations in real experiments.

2.4.3 Statistic Analysis

Spectral Analysis is used to get the variability of temperature, pH, and DO for all scenarios between 12 hours and 24 hours period. The spectral data are then integrated using trapezoid method to get the mean, and the 95% confidence interval. Bootstrap analysis is applied to the integrated exposure calculation for each variable of each specie. In order to assure a good dataset, 10000 iterations with replacement are done using a sample size of length equals half of the data used. The mean is calculated every time and saved. In the end, median, the confidence interval (CI) is calculated based on 2.5% percentile and 97.5 % percentile of the mean dataset.

2.5 Results

2.5.1 Model Comparison

To check model skill, spectral analyses were done on the temperature, DO, and pH time series (Figure 2.9). Model means for temperature and pH are not statistically different from what is observed in the *in situ* data. However, model mean oxygen is almost half of the observed mean from the data. The low mean value for oxygen could be due to the fact we are not fully representing the high primary productivity due to kelp forest environment (Reed et al., 2011). However, we are reproducing observed minimum values that would present a potential stressful condition for nearshore animals.

Frequencies occurring between peaks are not well resolved for the variables I examined. This could be because I am using a 2D model to study hypoxia and acidification, and therefore, am not able to have all the physical processes captured in the theoretical model. Moreover, these frequencies represent other processes happening in the coastal ocean, but do not have an appreciable effect on exposure calculations. For Monterey Bay diurnal (cpd=1) and semi diurnal (cpd=1.93) are the main components of variability, and therefore, are well represented and within the 95% confidence interval for temperature, oxygen and pH. It is worth pointing out that even higher frequencies such as cpd=3 and cpd=4 are also within the 95% confidence interval. Thus, the model is accurately simulating not only diurnal and semi diurnal cycles, but also other higher order tidal components (Woodson, 2013). Internal waves are observed in the model domain as vertical changes in the u-component of the velocity (Figure 2.9). Temperature profile is used rather than isopycnals as salinity is constant ($S=34$) throughout the water column. Internal waves generated bring the isotherms up and down close to the shore (not shown).

Also, cross-shelf velocity ranges from -0.05 to 0.1 m/s, and is within the range found in other studies (Carter, 2010; Walter et al., 2014; Kowek et al., 2017). Before the arrival of the internal wave crest, isotherms are tilted downwards indicating previous downwelling. An onshore patch of water occurs in between crests (between 0-15km) with opposite velocities. Opposite velocity between crests is also observed during retreating of internal waves in the

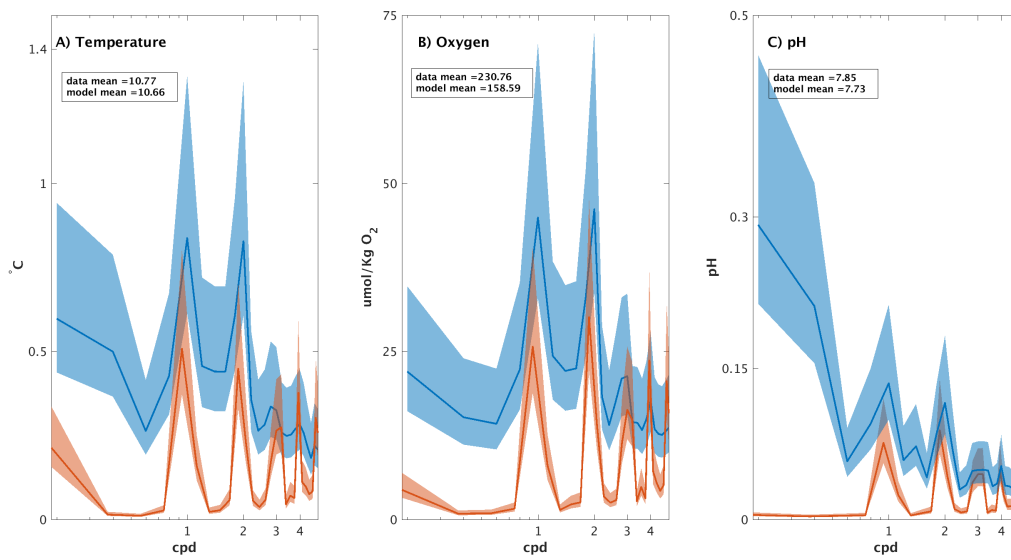


Figure 2.9: Power spectra of temperature (a), oxygen (b), and pH (c) from data used in (Booth et al., 2012) and current model showing model reproduces observed semi-diurnal and diurnal variability. Solid blue line represents the mean and the confidence intervals for the *in situ* data is represented by the blue line and shading, while solid red line represents our model output data with its confidence intervals (red shading). Data and model means are also shown.

domain, as it has been observed in studies on internal waves with in-situ data (Walter et al., 2014; Woodson, 2018).

Time series of temperature, oxygen, and pH, for present, RCP2.6, RCP4.5, RCP6.0, and RCP8.5 at 15 meter depth illustrate the high variability observed in all model runs (Figures 2.11, 2.12, and 2.13 respectively). The figures represent the 1 month window after the spin up period (not shown). Mean temperatures were 10.63°C (SD=0.39), 13.81°C (SD=0.46), 15.46°C (SD=0.50), 15.45°C (SD=0.49), 16.96°C (SD=0.95) for present, RCP 2.6, RCP 4.5, RCP 6.0, and RCP 8.5, respectively. Overall, the mean increased as expected and maintained about the same standard deviation (SD) across all RCPs except for RCP 8.5 scenario. This could be a combination of high temperature profile and high shortwave radiation imposed causing the surface water to be less dense than the others, and therefore, making the variability higher.

The means for dissolved oxygen are 5.15 mg/L (s=0.74) for present, 4.80 mg/L (SD=0.88) for RCP 2.6, 5.32 mg/L (SD=0.77) for RCP 4.5, 5.02 mg/L (SD=0.81) for RCP 6.0, and 4.93 mg/L (SD=1.21) for RCP 8.5. The standard deviation (SD) for RCP 8.5 shows almost double the variability compared to the other scenarios. This is likely due to a stronger gradient in oxygen (surface remains saturated while the values at depth are lower). It is worth pointing out that RCP 2.6 has the lowest mean and RCP 4.5 is 0.52 mg/L higher, but not significantly different than the present scenario. The consequence for the lowest mean DO in RCP 2.6 is possibly related to the low temperature stratification and associated low production of phytoplankton, and therefore, low oxygen at 15 meters. Another scenario (not shown) was used in order to prove that where RCP 4.5 oxygen profile was applied in RCP 2.6 and the same low oxygen values found previously were also found in the alternate run.

The pH variability was also high across all model runs (Figure 2.13). The mean value for pH ranges from 7.73 (SD=0.07) for present to 7.44 (SD=0.12) for the RCP 8.5 scenario. RCP 8.5 again had the highest range among all scenarios. Otherwise, the pH range was around 0.075. Also, RCP 8.5 shows a weak pH trend in the end of the 3 week window. These lower pHs for the most extreme scenarios have also been observed in large scale models (Kwiatkowski and Orr, 2018).

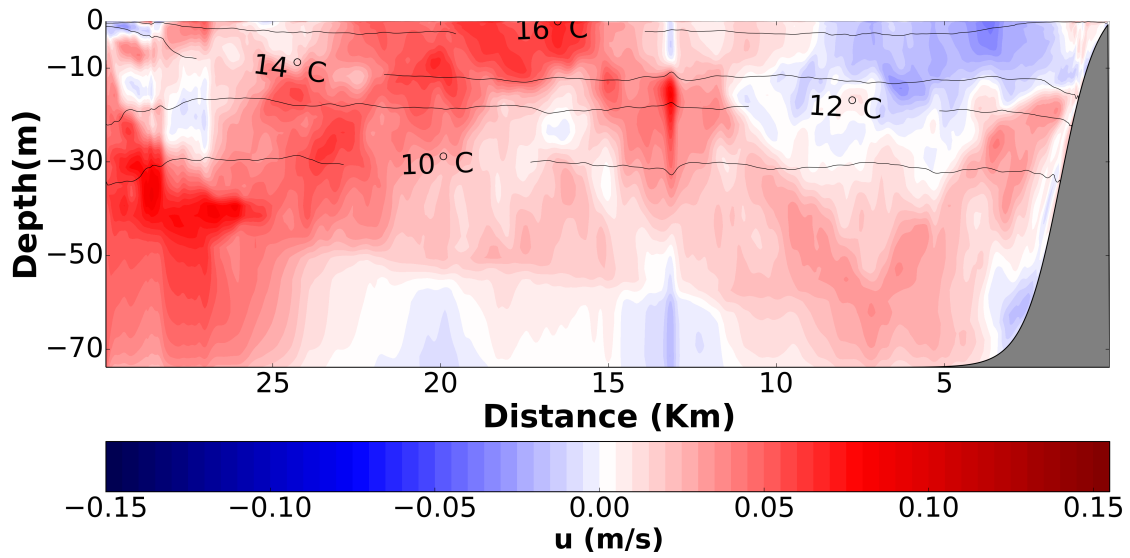


Figure 2.10: Snapshot of u-component of velocity and temperature on July, 6th 2013 from the model. Positive values are onshore, negative values are offshore. Contour lines (black) show isotherms with temperature labels.

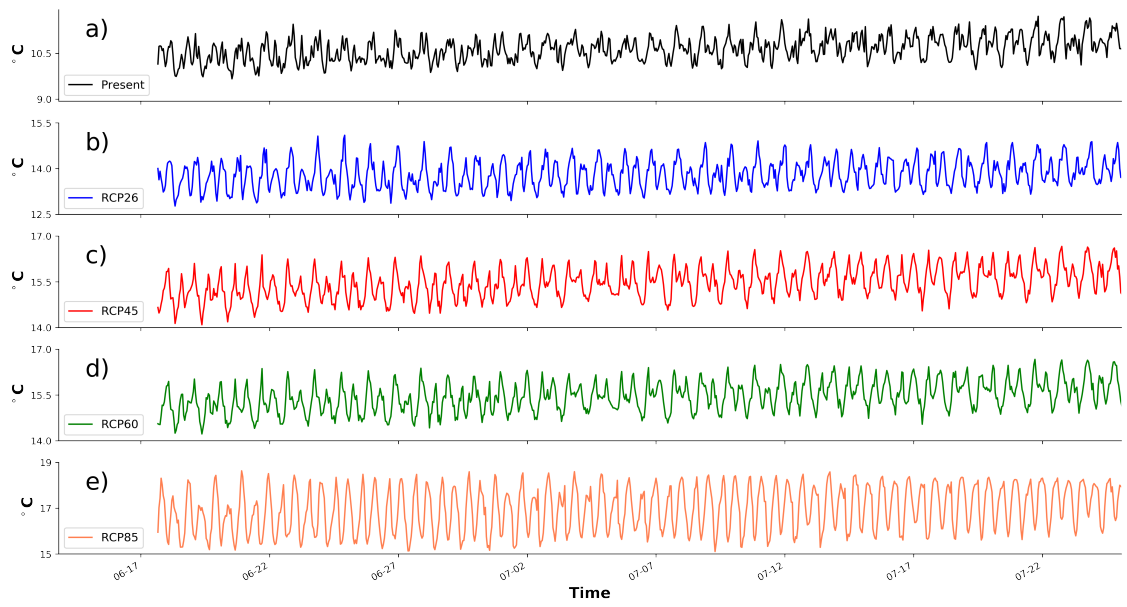


Figure 2.11: Modelled time series of Temperature for 1 month period with idealized upwelling for present day (a), RCP2.6 (b), RCP4.5 (c), RCP6.0 (d), and RCP8.5 (e).

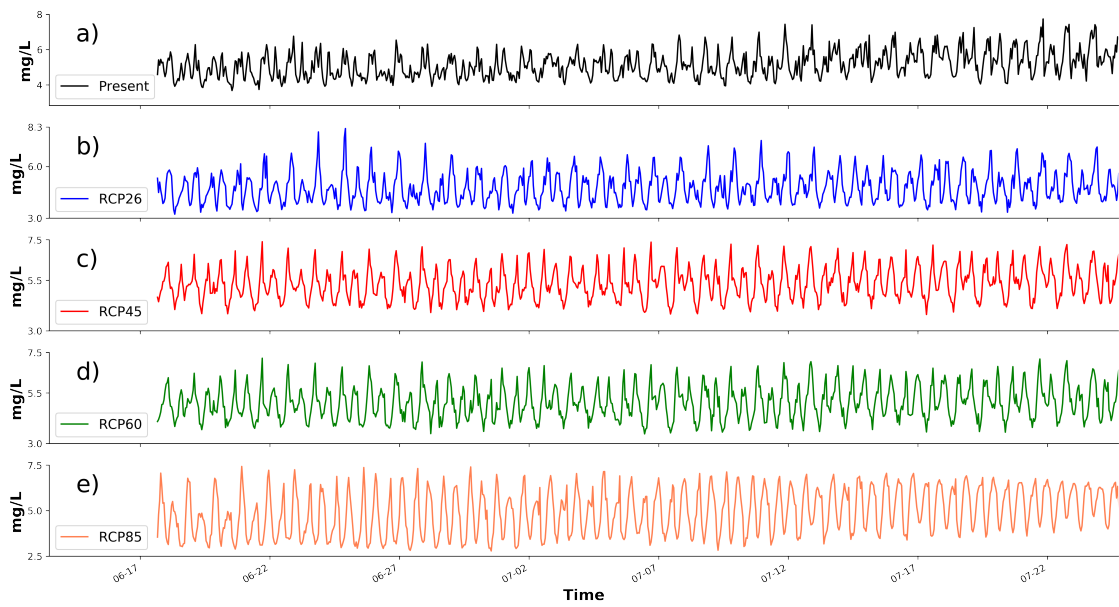


Figure 2.12: Modeled time series of O₂ for 1 month period with idealized upwelling present day (a), RCP2.6 (b), RCP4.5 (c), RCP6.0 (d), and RCP8.5 (e).

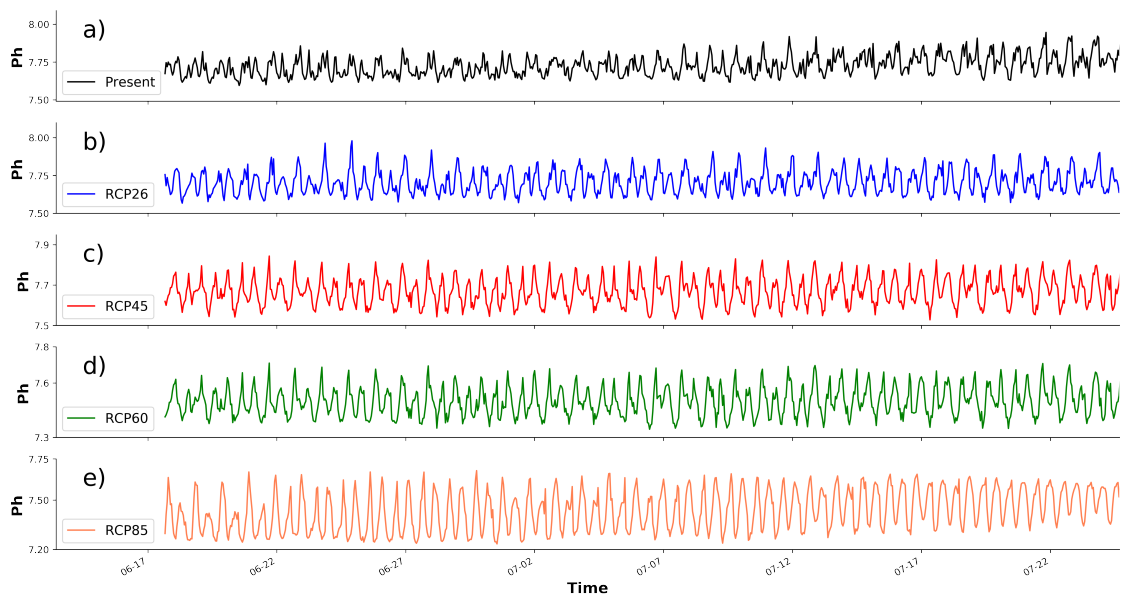


Figure 2.13: Modeled time series of pH for 1 month period with idealized upwelling Present day (a), RCP2.6 (b), RCP4.5 (c), RCP6.0 (d), and RCP8.5 (e).

2.5.2 Climate Change variability

Figure 2.14, shows daily variability that characterizes the differences between scenarios used in this study. In general, daily variability increases as pCO₂ increases in the atmosphere. The intensity as well as difference of daily variability are most pronounced in RCP 8.5 when compared to present for all variables. For temperature (Figure 2.14a), RCP 2.6 and Present are likely to be different. However, a significant difference is observed starting from RCP 4.5. The temperature variability range is the smallest in Present and mainly the same for RCP 2.6, RCP 4.5, and RCP 6.0.

On the other hand, oxygen daily variability shows that present and RCP 2.6 scenarios through 6.0 are significantly different (Figure 2.14b). Comparing the median and interquartile values for RCP 2.6 through 6.0 and present, I observe an increase in daily variability for RCP scenarios. However, this daily variability is not different when comparing among these 3 RCP scenarios. The spread of the data for each RCP is somewhat higher than present with the spread in the most extreme scenario double of that found in present conditions.

The only significant daily variability difference is RCP 8.5 when compared to present data for pH (Figure 2.14c). While I expected an increase in variability across the climate change scenarios daily, variability is similar up to RCP 6.0 and an increase is only seen for RCP 8.5. The increase between present day and RCPs 2.6 and 6.0 are not significant although there is an observed increase.

2.5.3 Integrated Exposure

Exposure to all stressors (pH, DO, temperature) is expected in future climate scenarios for both species and responses examined (Figure 2.15). In general, I observe a pattern where neither of species are exposed to any stress until RCP 4.5 scenario (Figure 2.15a). Also, RCP 8.5 has the highest daily exposure to temperature. Exposure to higher temperatures would be more intense for red abalone in all scenarios compared to the purple sea urchin. Daily mean exposure for red abalone in scenarios 4.5 and 6.0 are 5-fold more intense than the mean exposure of sea urchin for the same scenarios. This difference is about 1.5-fold when comparing the means of both species using RCP 8.5 scenario. The daily range of

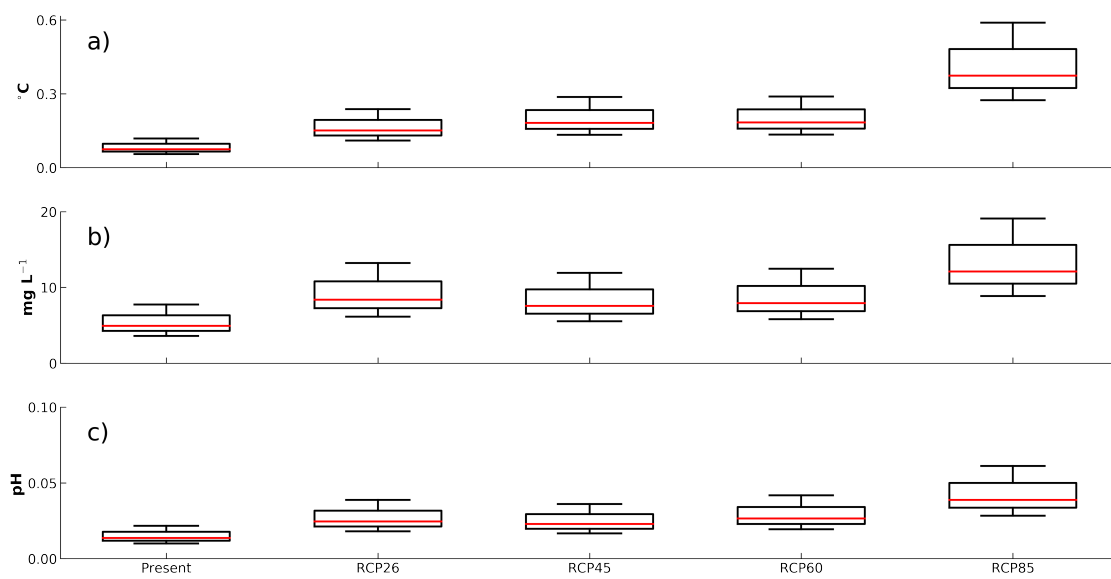


Figure 2.14: Integrated spectral daily variability for Temperature, DO, and pH. The y-axis gives the temperature, DO, and pH and the x-axis represents the scenarios. Red lines give the median of temperature, DO, and pH for each scenario. Whiskers represent the 95% confidence interval estimated using spectral analysis.

exposures to temperature are approximately the same between the two taxa. Daily exposure of *Haliotis rufescens* to stress is on average 0.11°C for RCP 2.6, 1.5°C for RCP 4.5 and 6.0, and approximately 3°C for RCP 8.5. This change represents almost a 3-fold increase on average in intensity from RCP 2.6 to RCP 8.5. Neither Present nor RCP 2.6 daily variability of temperature cause stress on fertilization of *Paracentrotus lividus* (Figure 2.15a). Exposure to extreme temperature may be a problem for scenarios RCP 4.5, 6.0, and 8.5 however. All scenarios represent a significant increase in exposure when compared to present and RCP 2.6. The highest daily exposures for RCP 4.5 and RCP 6.0 are approximately half of the lowest exposure that sea urchin would face in RCP 8.5 scenario.

Both species exhibit a stress to low oxygen for all scenarios (Figure 2.15b). In general, both species have the same trend and overall variability ($s=\pm 0.17$). Also, overall mean daily oxygen exposure is 0.81 mgL⁻¹ d for red abalone and 0.65 mgL⁻¹ d for sea urchin. RCP 2.6 and 8.5 are significant different than present conditions for fertilization of red abalone. With exception of Present and RCP 8.5, the difference between the lowest daily exposure of oxygen for red abalone and highest daily exposure of oxygen for sea urchin is approximately 0.08 mgL⁻¹ d. Daily exposure for scenarios 2.6, 4.5, and 6.0 have less variability than present and RCP 8.5 scenarios for both species. In addition, the lower 25% mean daily exposure to oxygen for present conditions for red abalone represents the same mean exposure as the higher 25 % mean daily exposure for present scenario for the purple sea urchin. Moreover, *H. rufescens* has the highest mean daily oxygen exposure for RCP 2.6 and RCP 8.5 scenarios among all scenarios and between species. On average, red abalone exhibit the same exposure as both the highest mean daily exposure in RCP 6.0 and lowest mean oxygen exposure in RCP 8.5 for sea urchin. Nevertheless, RCPs 4.5 and 6.0 are not significant different than present. In fact, the higher 25% mean daily exposure of oxygen in RCP 4.5 falls within the lower 25% mean daily exposure of oxygen in present scenario for red abalone. This situation repeats itself when comparing the higher 25% mean daily exposure for Present against the lower 25% mean daily found for RCP 6.0. Overall, RCP 8.5 has the largest variability in exposure to low oxygen over a day for an adult purple sea urchin. The amount of stress experienced by an adult purple sea urchin due to exposure to mean hypoxic waters in a day in RCP 6.0 scenario is about the same as the highest mean daily exposure caused for present.

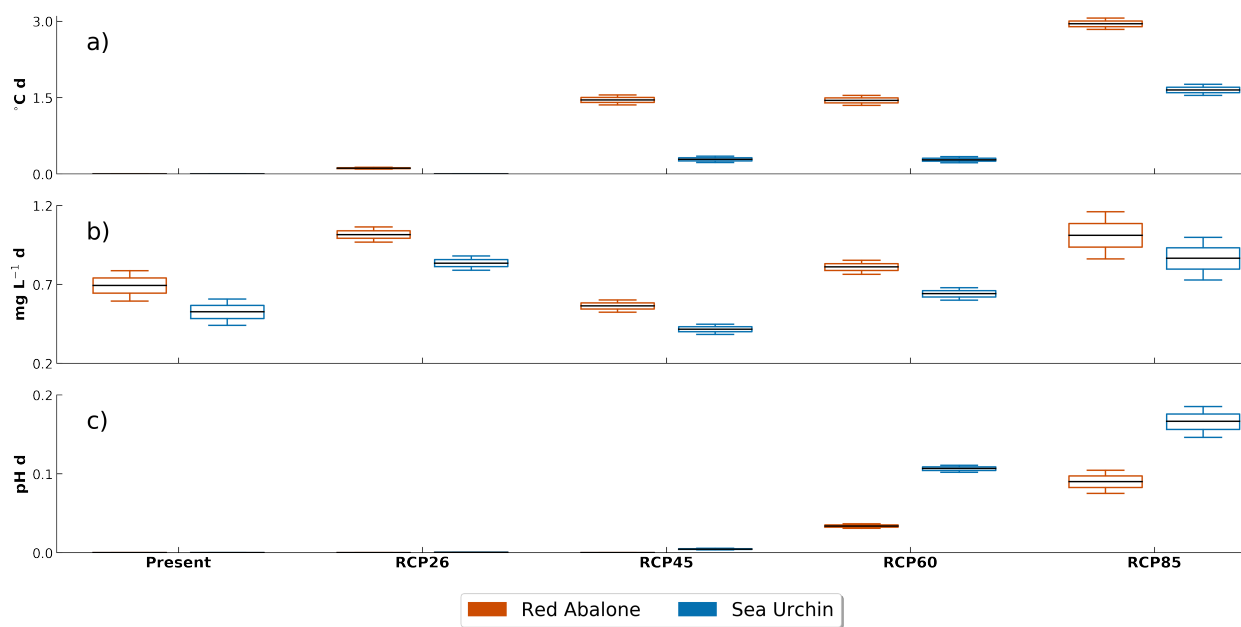


Figure 2.15: Bootstrap of the mean daily integrated exposure of temperature (a), dissolved oxygen (b), and acidification (c) from present and future scenarios for red abalone (*Haliotis rufescens*) and sea urchin (*Paracentrotus lividus* and *Mesocentrotus franciscanus*). Box plots show mean, 25% and 75% quantiles, and data range.

Exposure to low DO in RCP 6.0 is also roughly equivalent to the lowest mean daily exposure values in the RCP 8.5 scenario.

Overall, daily exposure to pH is significantly different only for the last two scenarios (Figure 2.15c). Purple sea urchins show on average a stronger daily exposure to pH in both scenarios than the strongest mean daily exposure for red abalone. Comparing the same RCP 6.0 scenarios for both species, the purple sea urchin is 3-fold more exposed to daily variability of pH than red abalone. This mean exposure decreases to 2-fold when comparing RCP 8.5 scenarios. Both RCP 6.0 and 8.5 scenarios for purple sea urchins are significantly different from Present, RCP 2.6, and RCP 4.5 (Figure 2.15c). The mean daily exposures are 0.10 pH d and 0.17 pH d for RCP 6.0 and RCP 8.5, respectively. The lowest daily pH exposure value for RCP 8.5 represents almost 1.3 times more than the highest daily exposure sea urchin would be exposed in RCP 6.0 scenario. The same trend across scenarios is also observed for red abalone. However, based on the threshold values used for pH, the fertilization stage of purple sea urchins appears to be more sensitive to pH stress than fertilization of red abalone. Even though red abalone has a higher threshold the difference between the highest value of RCP 6.0 and lowest value of RCP 8.5 is approximately 1.7-fold higher than the difference observed for purple sea urchins. Mean daily exposure to pH increases approximately 3-fold when comparing the mean daily values of RCP 6.0 and RCP 8.5 for *H. rufescens*.

2.6 Discussion

The 2D idealized model developed in this thesis examines the response of organisms to multiple stressors (temperature, hypoxia, acidification) for future scenarios in the nearshore region of Monterey Bay, CA. In Monterey Bay, significant variability in stressors occurs due to daily solar and tidal cycles (Woodson, 2013). Variability at the semi-diurnal tidal period is caused by internal tidal bores that enter the nearshore bringing with them cold, nutrient rich, but low in oxygen and pH, waters. The variability in the nearshore due to these processes can be larger than the total change in the stressors predicted via large-scale climate models. Using idealized tidal and wind patterns, the model captures variability in important stressors at diurnal and semi-diurnal (internal tides) frequencies observed in Monterey Bay for present conditions. Using the model with initial and forcing conditions expected under future climate scenarios, I found that stress to all variables increased in future conditions. Stress also increased as the RCP pathway (projected carbon dioxide emissions) increased from 2.6 to 8.5. However a few important, unexpected patterns emerged (Figure 2.15). First, for the two species examined (*H. rufescens* and *P. lividus*), exposure to extreme high temperatures or low pH did not occur below RCP 4.5, but did for low oxygen. Second, exposure to low oxygen generally did not increase across all scenarios with the only difference being the amount of exposure variability in RCP 8.5. Third, the increased variability in RCP 8.5 was observed across all stressors. Below, I discuss some of the ramifications of these patterns in the context of large-scale climate change and what these results may portend for nearshore ecosystems in the future. I also discuss how experiments may be designed to mimic model results and provide insights into organism and community responses to future climate conditions.

One important observation is the difference in the mean values for oxygen between the present model and observations. Mean values of oxygen are lower in the model by $80 \mu\text{mol kg}^{-1}$. This difference is likely because the region in study is located in a high primary productivity environment due to the presence of dense kelp forests. At this point, I was not able to simulate the extremely high primary productivity (and consequent oxygen production) associated with kelp using ROMS. Importantly however, our estimates of oxygen

variability and exposure agree with estimates from present observations. On the other hand, temperature and pH mean values are in accordance with *in situ* data for the region. Moreover, cross-shelf velocity is within the values found in other studies (Carter, 2010; Walter et al., 2014; Koweeck et al., 2017).

Projections from the model suggest that the southern region of Monterey Bay, CA will have a slight increasing trend in exposure for temperature, oxygen, and pH in daily variability for all climate change scenarios. By applying the same transport and mixing and finding similar variability in stressors for present conditions in Monterey Bay, CA, I was able to quantify how temperature, oxygen, and pH would vary at 15 meters water depth. The model is used to estimate the stress for two important kelp forest species based on laboratory estimated thresholds for fertilization in future scenarios. At 15 meters, mean temperature follows the trend found in studies on the west coast (Feely et al., 2018) as well as at the surface in large-scale models (Bopp et al., 2013). In contrast, mean pH shows a decrease of 0.48 from present to RCP 8.5. This change is consistent with values found for surface in regional(Gruber et al., 2012) and large scale models(Bopp et al., 2013) for the region. Interaction of internal tides and a warmer water column in the nearshore environments contribute to strengthening/development of a more stratified waters in the future simulations (Laurent et al., 2018; Woodson, 2018). A more intense stratification and higher temperatures promote a decrease in bottom oxygen in regional models (Meire et al., 2013; Laurent et al., 2018). This decline is also observed for the mean oxygen for future scenarios with exception of RCP 4.5 when compared to present for the model results. The lowest value found for RCP 2.6 and highest found for RCP 4.5 demonstrate the high variability and complexity of the nearshore environment.

Overall, red abalone appears to be more sensitive to daily temperature and oxygen exposures in this region. In contrast, a higher threshold to pH for sea urchin fertilization makes it more susceptible to acidification when compared to red abalone. When calculating exposure using mean surface values of temperature, O₂, and pH for RCP 8.5, exposure for the same organisms is estimated to be much higher than the actual exposure calculated based on the nearshore model. For example RCP 8.5 projects temperatures of 19°C yielding a daily exposure of 5°C d for *H. rufescens* (Table 2.4) compared to approximately 3°C d. Similarly,

integrated exposure to low oxygen and pH would be about $1 \text{ mgL}^{-1} \text{ d}$ and 0.24 pH d as opposed to $5.25 \text{ mgL}^{-1} \text{ d}$ and 0.1 pH d respectively based on large-scale climate projections. Overall exposure of nearshore ecosystems to these three important climate stressors will therefore be significantly lower than projected by large-scale climate models with significant exposure beyond natural variability not occurring below RCP 4.5 or even RCP 6.0.

The observed differences in exposure translate to even larger differences in fertilization rate. Table 2.7 shows the proportional fertilization and exposure to pH and DO for 3 different cases for RCP8.5: Non-upwelling, upwelling, and nearshore model. Non-upwelling values are the surface values at the surface used in our initialization (surface values from appropriate CMIP5 RCP). Upwelling values for the CMIP5 model are taken as the bottom values used in the input profiles in the present model. Bottom values are derived from 200 m water depth in RCP8.5 projections as this is a common depth for upwelling source waters in the central California Current region. For 2D model, mean pH and DO for RCP 8.5 at 15 meters are used. Proportional fertilization is based on the estimated pH and temperature for each case. We observe a pattern based on temperature where there is an increase in proportional fertilization as the temperature increases. This relationship is not immediately clear when making a comparison between the mean pH from different scenarios. Interestingly, there is no accumulated exposure for the non-upwelling scenario in RCP 8.5. In contrast, the upwelling case has accumulated exposure over 200% greater than the same scenario when using an idealized model for nearshore ecosystem. The results for exposure of pH show that my model would exhibit the same accumulated exposure as CMIP5 upwelling over (1 week) only after a 3 week period with the maximum daily exposure found for pH previously. Therefore, using CMIP5 values in laboratory would either overstress or not stress the organisms at all. Estimating the accumulated exposure to pH using (Boch et al., 2017) produces an accumulated exposure between RCP 4.5 and 6.0 in the 2D nearshore model. No stress to exposure would be found if using non-upwelling scenario. Mean oxygen is similar between CMIP5 (upwelling) and present upwelling scenarios (Boch et al., 2017) since extreme low oxygen values presently observed in Monterey Bay. These results suggest that both scenarios may be over-stressing the red abalone fertilization beyond what is likely expected in future climate change.

Table 2.7: Comparison different scenarios of accumulative exposure to acidification and hypoxia during a period of a week for *H. rufescens*.

	mean pH	mean O ₂ (mg L ⁻¹)	mean Temp (°C)	Prop. Fert.*	Exposure**	
					pH d	mg L ⁻¹ d
CMIP5 (RCP 8.5) (non-upwelling)	7.79	7.25	19	0.5	0	0
CMIP5 (RCP 8.5) (upwelling)	7.2	2	10.81	0.29	2.1	26.04
2D model	7.44	4.93	17	0.4	0.63	7.07

*Proportional Fertilization interpolated based on figure 4 from Boch et al. (2017).

**Thresholds for red abalone (Table 2.6) used in order to calculate exposure for pH and DO.

Modeling of daily exposure for upwelling environment driven by internal tides using high temporal and spatial resolution is computationally costly. Consequently, an idealized 2D model can be applied to simulate variability of temperature, oxygen and pH in the nearshore environment. This could ensure robustness by giving support to the variability observed and variability we might observe for warming, hypoxia, and acidification scenarios in ocean-mimicking tanks (Cressey, 2015).

2.7 Conclusions

Based on the model output, daily variability in Monterey Bay will increase across climate change scenarios. However, this increase will not be significantly different than the variability observed for present. The only exception is RCP 8.5 scenario that presents a significant increase in daily variability for all variables. Benthic organisms such as abalone and urchins would start showing signs of stress only in scenarios 6.0 and 8.5 for temperature, and 4.5 and on for pH. Daily oxygen exposure would be the only variable that shows stress for all scenarios demonstrating the sensitivity of organisms to hypoxia and the occurrence of naturally low oxygen waters already present. Based on model results, laboratory experiments in order to measure the effects of climate change scenarios on benthic organisms should must include natural or even increased variability to reflect the natural environment.

Chapter 3

Final Remarks and Future directions

Exposure to acidic, hypoxic and warmer waters is going to affect the nearshore organisms in future climate conditions. The question is how large-scale climate change impacts will translate into a stress for nearshore organisms and the communities and ecosystems that they inhabit. A key factor in determining these local-scale impacts is understanding how the high frequency variability will change from present to future climate change scenarios. Some laboratory experiments have started using natural variability to understand how fluctuations will affect the exposure of these organisms to stressful conditions. However, these daily exposure calculations can only be done using present *in situ* data since IPCC models only have coarse temporal and spatial resolution. In this study I built a 2D idealized model with biological components for Monterey Bay, as an example, to try to understand how pH, DO, and temperature are going to change in the future for an environment forced by winds, tides, and internal tides. I tested the skill of the model at representing the variability caused by diurnal and semi-diurnal periods in pH, dissolved oxygen, and temperature. I observed that the model is not perfect for not representing the "real world"; however, it represented current conditions well enough that we could apply it to future climate scenarios and examine exposure to these stressors. Two benthic species and their respective threshold for fertilization rate and adult grazing were chosen to demonstrate their respective difference among scenarios and how my model improves estimates of daily exposure calculated using large scale models. Thus, I found the following results:

- Mean temperatures increase as the scenarios get warmer. Mean oxygen does not follow a pattern of increasing as the scenarios get warmer. However, mean pH decreases from

Present to RCP 8.5 scenario.

- There is no sign of a strengthening in daily variability except for the most IPCC extreme scenario.
- Red abalone and sea urchin will likely be exposed to daily stress for all variables in the future.
- Daily exposure to temperature only would be significant from RCP 4.5 scenario and on.
- All scenarios of DO daily exposure are going to cause some stress.
- These organisms would not be under pH stress until either RCP 6.0 or 8.5 occur.
- Calculated exposure using large scale models either over-or underestimate stress on nearshore organisms. The use of these large scale model outputs would bias the laboratory studies.
- The results showed in Table 2.7 demonstrate the use of my model as a comparison from static laboratory experiments to other benthic organisms.

This model is just one step towards a better understanding of how climate change scenarios would play out for different organisms, especially benthic organisms. Thus, next steps are needed:

- Add time varying drag coefficient to mimic kelp forest growth and death.
- Adjust the production of primary productivity associated with kelp forests in the model.
- Build a more realistic three-dimensional model for the region of Monterey Bay, CA.

Bibliography

- Boch, C. A., S. Y. Litvin, F. Micheli, G. De Leo, E. A. Aalto, C. Lovera, C. Brock Woodson, S. Monismith, J. P. Barry, and (2017). Effects of current and future coastal upwelling conditions on the fertilization success of the red abalone (*haliotis rufescens*). *ICES Journal of Marine Science* 74(4), 1125–1134.
- Boch, C. A., F. Micheli, M. Alnajjar, S. G. Monismith, J. M. Beers, J. C. Bonilla, A. M. Espinoza, L. Vazquez-Vera, and C. B. Woodson (2018). Local oceanographic variability influences the performance of juvenile abalone under climate change. *Scientific Reports* 8(1), 1–12.
- Bograd, S. J., C. G. Castro, E. Di Lorenzo, D. M. Palacios, H. Bailey, W. Gilly, and F. P. Chavez (2008). Oxygen declines and the shoaling of the hypoxic boundary in the California Current. *Geophysical Research Letters* 35(12), 1–6.
- Booth, J. A. T., E. E. McPhee-Shaw, P. Chua, E. Kingsley, M. Denny, R. Phillips, S. J. Bograd, L. D. Zeidberg, and W. F. Gilly (2012). Natural intrusions of hypoxic, low pH water into nearshore marine environments on the California coast. *Continental Shelf Research* 45, 108–115.
- Bopp, L., L. Resplandy, J. C. Orr, S. C. Doney, J. P. Dunne, M. Gehlen, P. Halloran, C. Heinze, T. Ilyina, R. Séférian, J. Tjiputra, and M. Vichi (2013). Multiple stressors of ocean ecosystems in the 21st century: Projections with CMIP5 models. *Biogeosciences* 10(10), 6225–6245.
- Breaker, L. and W. Broenkow (1994). The circulation of Monterey Bay and Related Processes. *Oceanography and Marine Biology* 32, 1–64.
- Cabré, A., I. Marinov, R. Bernardello, and D. Bianchi (2015). Oxygen minimum zones in the tropical Pacific across CMIP5 models: Mean state differences and climate change trends. *Biogeosciences* 12(18), 5429–5454.
- Carter, G. S. (2010). Barotropic and Baroclinic M 2 Tides in the Monterey Bay Region. *Journal of Physical Oceanography* 40, 1766–1783.
- Chan, F., J. A. Barth, C. A. Blanchette, R. H. Byrne, F. Chavez, O. Cheriton, R. A. Feely, G. Friederich, B. Gaylord, T. Gouhier, S. Hacker, T. Hill, G. Hofmann, M. A. McManus, B. A. Menge, K. J. Nielsen,

- A. Russell, E. Sanford, J. Sevadjian, and L. Washburn (2017). Persistent spatial structuring of coastal ocean acidification in the California Current System. *Scientific Reports* 7(1), 1–7.
- Chavez, F. P. and M. Messié (2009). A comparison of Eastern Boundary Upwelling Ecosystems. *Progress in Oceanography* 83(1-4), 80–96.
- Checkley, D. M. and J. A. Barth (2009). Patterns and processes in the California Current System. *Progress in Oceanography* 83(1-4), 49–64.
- Connell, S. D. and B. D. Russell (2010). The direct effects of increasing CO₂ and temperature on non-calcifying organisms: increasing the potential for phase shifts in kelp forests. *Proceedings of the Royal Society B: Biological Sciences* 277(1686), 1409–1415.
- Cressey, D. (2015). Seawater studies come up short. *Nature* 524, 18–19.
- Dettner, A., H. L. Swinney, and M. S. Paoletti (2013). Internal wave and boundary current generation by tidal flow over topography. *Physics of Fluids* 25(2013).
- Deutsch, C., H. Brix, T. Ito, and L. Thompson (2011). Climate-Forced Variability of Ocean Hypoxia. *Science* 333(July), 336–339.
- Diaz, R. J. and R. Rosenberg (2008). Spreading dead zones and consequences for marine ecosystems. *Science* 321(5891), 926–929.
- Dickson, A. G. (1990). Standard potential of the reaction: $\text{AgCl(s)} + 1/2 \text{H}_2(\text{g}) = \text{Ag(s)} + \text{HCl(aq)}$, and the standard acidity constant of the ion HSO_4^- in synthetic sea water from 273.15 to 318.15 K. *Journal of Chemical Thermodynamics* 22(2), 113–127.
- Dickson, A. G. and F. J. Millero (1987). A comparison of the equilibrium constants for the dissociation of carbonic acid in seawater media. *Deep Sea Research Part A, Oceanographic Research Papers* 34(10), 1733–1743.
- Doney, S. C. (2010). The Growing Human Footprint on Coastal and Open-Ocean Biogeochemistry. *Science* 328(5985), 1512–1516.
- Doney, S. C., V. J. Fabry, R. A. Feely, and J. A. Kleypas (2009). Ocean Acidification: The Other CO₂ Problem.
- Feely, R. A., R. R. Okazaki, W. J. Cai, N. Bednaršek, S. R. Alin, R. H. Byrne, and A. Fassbender (2018). The combined effects of acidification and hypoxia on pH and aragonite saturation in the coastal waters of the California current ecosystem and the northern Gulf of Mexico. *Continental Shelf Research* 152(August), 50–60.

- Fennel, K., J. Wilkin, J. Levin, J. Moisan, J. O'Reilly, and D. Haidvogel (2006). Nitrogen cycling in the Middle Atlantic Bight: Results from a three-dimensional model and implications for the North Atlantic nitrogen budget. *Global Biogeochemical Cycles* 20(3), 1–14.
- Fennel, K., J. Wilkin, M. Previdi, and R. Najjar (2008). Denitrification effects on air-sea CO₂ flux in the coastal ocean: Simulations for the northwest North Atlantic. *Geophysical Research Letters* 35(24), 1–5.
- Frieder, C. A., J. P. Gonzalez, E. E. Bockmon, M. O. Navarro, and L. A. Levin (2014). Can variable pH and low oxygen moderate ocean acidification outcomes for mussel larvae? *Global Change Biology* 20(3), 754–764.
- Gangopadhyay, A., P. F. Lermusiaux, L. Rosenfeld, A. R. Robinson, L. Calado, H. S. Kim, W. G. Leslie, and P. J. Haley (2011). The California Current System: A multiscale overview and the development of a feature-oriented regional modeling system (FORMS). *Dynamics of Atmospheres and Oceans* 52(1-2), 131–169.
- García-Reyes, M., W. J. Sydeman, D. S. Schoeman, R. R. Rykaczewski, B. A. Black, A. J. Smit, and S. J. Bograd (2015). Under Pressure: Climate Change, Upwelling, and Eastern Boundary Upwelling Ecosystems. *Frontiers in Marine Science* 2(December), 1–10.
- Garrett, C. (2003). Internal tides and ocean mixing. *Science* 301(5641), 1858–1859.
- Gobler, C. J. and H. Baumann (2016). Hypoxia and acidification in ocean ecosystems: coupled dynamics and effects on marine life. *Biology letters* 1.
- Gobler, C. J., H. R. Clark, A. W. Griffith, and M. W. Lusty (2017). Diurnal Fluctuations in Acidification and Hypoxia Reduce Growth and Survival of Larval and Juvenile Bay Scallops (*Argopecten irradians*) and Hard Clams (*Mercenaria mercenaria*). *Frontiers in Marine Science* 3(January), 1–12.
- Gobler, C. J., E. L. DePasquale, A. W. Griffith, and H. Baumann (2014). Hypoxia and acidification have additive and synergistic negative effects on the growth, survival, and metamorphosis of early life stage bivalves. *PLoS ONE* 9(1).
- Graham, H., S. P. S. Rastrick, H. S. Findlay, M. G. Bentley, S. Widdicombe, A. S. Clare, and G. S. Caldwell (2016). Sperm motility and fertilisation success in an acidified and hypoxic environment. *ICES Journal of Marine Science* 73(3), 783–790.
- Graham, M. H. (2004). Effects of Local Deforestation on the Diversity and Structure of Southern California Giant Kelp Forest Food Webs. *Ecosystems* 7(4), 341–357.
- Graham, W. M., J. G. Field, and D. C. Potts (1992). Persistent "upwelling shadows" and their influence on zooplankton distributions. *Marine Biology* 114(4), 561–570.

- Graham, W. M. and J. L. Largier (1997). Upwelling shadows as nearshore retention sites: The example of northern Monterey Bay. *Continental Shelf Research* 17(5), 509–532.
- Gruber, N., C. Hauri, Z. Lachkar, and D. Loher (2012). Rapid Progression of Ocean Acidification in the California Current System /. 4(June), 1–5.
- Haidvogel, D. B., H. Arango, W. P. Budgell, B. D. Cornuelle, E. Curchitser, E. Di Lorenzo, K. Fennel, W. R. Geyer, A. J. Hermann, L. Lanerolle, J. Levin, J. McWilliams, A. J. Miller, A. M. Moore, T. Powell, A. F. Shchepetkin, and J. Wilkin (2008). Ocean forecasting in terrain-following coordinates: Formulation and skill assessment of the Regional Ocean Modeling System. *Journal of Computational Physics* 227, 3595–3624.
- Hofmann, G. E., J. E. Smith, K. S. Johnson, U. Send, L. A. Levin, F. Micheli, A. Paytan, N. N. Price, B. Peterson, Y. Takeshita, P. G. Matson, E. de Crook, K. J. Kroeker, M. C. Gambi, E. B. Rivest, C. A. Frieder, P. C. Yu, and T. R. Martz (2011). High-frequency dynamics of ocean pH: A multi-ecosystem comparison. *PLoS ONE* 6(12).
- Huyer, A. (1983). Coastal upwelling in the California current system. *Progress in Oceanography* 12(3), 259–284.
- IPCC (2013). *Summary for Policymakers*. Cambridge, United Kingdom and New York, NY, USA: Cambridge University Press.
- Kämpf, J. and P. Chapman (2016). *Upwelling Systems of the World*.
- Karstensen, J., L. Stramma, and M. Visbeck (2008). Oxygen minimum zones in the eastern tropical Atlantic and Pacific oceans. *Progress in Oceanography* 77, 331–350.
- Koweek, D. A., K. J. Nickols, P. R. Leary, S. Y. Litvin, T. W. Bell, T. Luthin, S. Lummis, D. A. Mucciarone, and R. B. Dunbar (2017). A year in the life of a central California kelp forest: Physical and biological insights into biogeochemical variability. *Biogeosciences* 14(1), 31–44.
- Krause-Jensen, D., N. Marba, M. Sanz-Martin, I. E. Hendriks, J. Thyrring, J. Carstensen, M. K. Sejr, and C. M. Duarte (2016). Long photoperiods sustain high pH in Arctic kelp forests. *Science Advances* 2(12), e1501938–e1501938.
- Kwiatkowski, L. and J. C. Orr (2018). Diverging seasonal extremes for ocean acidification during the twenty-first century. *Nature Climate Change* 8(2), 141.
- Laurent, A., K. Fennel, D. S. Ko, and J. Lehrter (2018). Climate Change Projected to Exacerbate Impacts of Coastal Eutrophication in the Northern Gulf of Mexico. *Journal of Geophysical Research: Oceans*, 3408–3426.

- Leary, P. R., C. B. Woodson, M. E. Squibb, S. G. Monismith, F. Micheli, and M. W. Denny (2017). “Internal tide pools” prolong kelp forest hypoxic events. *Limnology and Oceanography* 62(6), 2864–2878.
- Lewis, E. and D. Wallace (1998). Program Developed for CO2 system calculations. Technical report.
- Liu, G., S. F. Heron, C. M. Eakin, F. E. Muller-karger, M. Vega-rodriguez, L. S. Guild, J. L. D. L. Cour, E. F. Geiger, W. J. Skirving, T. F. R. Burgess, A. E. Strong, A. Harris, E. Maturi, A. Ignatov, J. Sapper, J. Li, and S. Lynds (2014). Reef-Scale Thermal Stress Monitoring of Coral Ecosystems: New 5-km Global Products from NOAA Coral Reef Watch. *Remote Sensing* (6), 11579–11606.
- Low, N. H. and F. Micheli (2018). Lethal and functional thresholds of hypoxia in two key benthic grazers. *Marine Ecology Progress Series* 594, 165–173.
- Marchesiello, P., J. C. McWilliams, A. Shchepetkin, P. Physics, and L. Angeles (2003). Equilibrium Structure and Dynamics of the California Current System. *Journal of Physical Oceanography* 33(4), 753–783.
- Martini, K., M. Alford, E. Kunze, S. Kelly, and J. Nash (2012). Internal Bores and Breaking Internal Tides on the Oregon Continental Slope. *Journal of Physical Oceanography* 43, 120–139.
- McClatchie, S., R. Goericke, R. Cosgrove, G. Auad, and R. Vetter (2010). Oxygen in the Southern California Bight: Multidecadal trends and implications for demersal fisheries. *Geophysical Research Letters* 37(19), 1–5.
- Meire, L., K. E. R. Soetaert, and F. J. R. Meysman (2013). Impact of global change on coastal oxygen dynamics and risk of hypoxia. *Biogeosciences* 10(4), 2633–2653.
- Micheli, F., A. Saenz-Arroyo, A. Greenley, L. Vazquez, J. A. Espinoza Montes, M. Rossetto, and G. A. de Leo (2012). Evidence that marine reserves enhance resilience to climatic impacts. *PLoS ONE* 7(7).
- Miller, R. J., D. C. Reed, and M. A. Brzezinski (2011). Partitioning of primary production among giant kelp (*Macrocystis pyrifera*), understory macroalgae, and phytoplankton on a temperate reef. *Limnology and Oceanography* 56(1), 119–132.
- Moulin, L., A. I. Catarino, T. Claessens, and P. Dubois (2011). Effects of seawater acidification on early development of the intertidal sea urchin *Paracentrotus lividus* (Lamarck 1816). *Marine Pollution Bulletin* 62(1), 48–54.
- Nelson, C. (1976). Wind stress and wind stress curl over the California Current. *Pacific Environmental Group, National Fisheries Service, National Oceanic and Atmospheric Administration, Technical Report* 714(1963), 89.

- Orr, J. C., V. J. Fabry, O. Aumont, L. Bopp, S. C. Doney, R. A. Feely, A. Gnanadesikan, N. Gruber, A. Ishida, F. Joos, R. M. Key, K. Lindsay, E. Maier-Reimer, R. Matear, P. Monfray, A. Mouchet, R. G. Najjar, G. K. Plattner, K. B. Rodgers, C. L. Sabine, J. L. Sarmiento, R. Schlitzer, R. D. Slater, I. J. Totterdell, M. F. Weirig, Y. Yamanaka, and A. Yool (2005). Anthropogenic ocean acidification over the twenty-first century and its impact on calcifying organisms. *Nature* 437(7059), 681–686.
- Reed, D. C., A. Rassweiler, K. C. Cavanaugh, and D. A. Siegel (2011). Wave disturbance overwhelms top-down and bottom-up control of primary production in California kelp forests. *Ecology* 92(11), 2108–2116.
- Ren, A. S., F. Chai, H. Xue, D. M. Anderson, and F. P. Chavez (2018). A Sixteen-year Decline in Dissolved Oxygen in the Central California Current. *Scientific Reports* 8(1), 1–9.
- Resplandy, L., L. Bopp, J. C. Orr, and J. P. Dunne (2013). Role of mode and intermediate waters in future ocean acidification: Analysis of CMIP5 models. *Geophysical Research Letters* 40(12), 3091–3095.
- Rosenfeld, L. K., F. B. Schwing, N. Garfield, and D. E. Tracy (1994). Bifurcated flow from an upwelling source: a cold water source for Monterey Bay. *Cont. Shelf Res.* 14(9), 931–964.
- Schuckmann, K. V., P.-y. L. Traon, E. Alvarez-fanjul, L. Axell, M. Balmaseda, L.-a. Breivik, R. J. W. Brewin, C. Bricaud, M. Drevillon, Y. Drillet, C. Dubois, O. Embury, H. Etienne, M. G. Sotillo, G. Garric, F. Gasparin, E. Gutknecht, S. Guinehut, F. Hernandez, M. Juza, B. Karlson, G. Korres, J.-f. Legeais, B. Levier, V. S. Lien, R. Morrow, G. Notarstefano, L. Parent, Á. Pascual, B. Pérez-gómez, C. Perruche, N. Pinardi, A. Pisano, P.-m. Poulain, I. M. Pujol, R. P. Raj, U. Raudsepp, H. Roquet, A. Samuelson, S. Sathyendranath, J. She, S. Simoncelli, C. Solidoro, J. Tinker, J. Tintoré, L. Viktorsson, M. Ablain, E. Almroth-rosell, A. Bonaduce, E. Clementi, G. Cossarini, Q. Dagneaux, C. Desportes, S. Dye, C. Fratianni, S. Good, E. Greiner, J. Gourrion, M. Hamon, J. Holt, P. Hyder, J. Kennedy, F. Manzano-muñoz, A. Melet, B. Meyssignac, S. Mulet, B. B. Nardelli, E. O. Dea, E. Olason, A. Paulmier, I. Pérez-gonzález, R. Reid, M.-f. Racault, D. E. Raitsos, A. Ramos, P. Sykes, T. Szekely, and N. Verbrugge (2016). The Copernicus Marine Environment Monitoring Service Ocean State Report. *Journal of Operational Oceanography* 9, 1755–8778.
- Stramma, L., G. C. Johnson, J. Sprintall, and V. Mohrholz (2008). Expanding Oxygen-Minimum Zones in the Tropical Oceans. *Science* 2006(May), 655–659.
- Suanda, S. H., J. A. Barth, and C. B. Woodson (2011). Diurnal heat balance for the northern Monterey Bay inner shelf. *Journal of Geophysical Research: Oceans* 116(9), 1–13.

- Talley, L. D., G. L. Pickard, Emery. William J., and J. H. Swift (2011). *Descriptive Physical Oceanography - An Introduction* (Sixth ed.).
- Tseng, Y. H., D. E. Dietrich, and J. H. Ferziger (2005). Regional circulation of the Monterey Bay region: Hydrostatic versus nonhydrostatic modeling. *Journal of Geophysical Research C: Oceans* 110(9), 1–21.
- Tsujino, H. and N. Suginohara (1998). Thermohaline effects on upper layer circulation of the North Pacific. *Journal of Geophysical Research* 103, 665–679.
- Vaquer-Sunyer, R. and C. M. Duarte (2008). Thresholds of hypoxia for marine biodiversity. *Proceedings of the National Academy of Sciences* 105(40), 15452–15457.
- von Dassow, P., F. Díaz-rosas, E. M. Bendif, D. Mella-flores, S. Rokitta, U. John, and R. Torres (2018). Overcalcified forms of the coccolithophore *Emiliania huxleyi* in high CO₂ waters are not pre-adapted to ocean acidification. *Biogeosciences Discussions* (March), 1–28.
- Walter, R. K., C. B. Woodson, P. R. Leary, and S. G. Monismith (2014). Connecting wind-driven upwelling and offshore stratification to nearshore internal bores and oxygen variability. *Journal of Geophysical Research: Oceans* 119(6), 3517–3534.
- Woodson, C. B. (2013). Spatiotemporal Variation in Cross-Shelf Exchange across the Inner Shelf of Monterey Bay, California. *Journal of Physical Oceanography* 43(8), 1648–1665.
- Woodson, C. B. (2018). The fate and impact of internal waves in nearshore ecosystems. *Annual Review of Marine Science* 10(1), 421–441. PMID: 28796571.
- Woodson, C. B., D. I. Eerkes-Medrano, A. Flores-Morales, M. M. Foley, S. K. Henkel, M. Hessian-Lewis, D. Jacinto, L. Needles, M. T. Nishizaki, J. O’Leary, C. E. Ostrander, M. Pespenti, K. B. Schwager, J. A. Tyburczy, K. A. Weersing, A. R. Kirincich, J. A. Barth, M. A. McManus, and L. Washburn (2007). Local diurnal upwelling driven by sea breezes in northern Monterey Bay. *Continental Shelf Research* 27(18), 2289–2302.
- Xiu, P., F. Chai, E. N. Curchitser, and F. S. Castruccio (2018). Future changes in coastal upwelling ecosystems with global warming: The case of the California Current System. *Scientific Reports* 8(1), 1–9.